

# Liquid jet in a high Mach number air stream

T.Funada,\* D.D.Joseph<sup>†‡</sup> M.Saitoh\* & S.Yamashita\*

\*Department of Digital Engineering, Numazu College of Technology, Ooka 3600, Numazu, Shizuoka, 410-8501 Japan

<sup>†</sup>Department Aerospace Engineering and Mechanics, University of Minnesota, Minneapolis, MN 55455, USA

## Abstract

The instability of circular liquid jet immersed in a coflowing high velocity airstream is studied assuming that the flow of the viscous gas and liquid is irrotational. The basic velocity profiles are uniform and different. The instabilities are driven by Kelvin-Helmholtz instability due to a velocity difference and neckdown due to capillary instability. Capillary instabilities dominate for large Weber numbers. Kelvin-Helmholtz instability dominates for small Weber numbers. The wave length for the most unstable wave decreases strongly with the Mach number and attains a very small minimum when the Mach number is somewhat larger than one. The peak growth rates are attained for axisymmetric disturbances ( $n = 0$ ) when the viscosity of the liquid is not too large. The peak growth rates for the first asymmetric mode ( $n = 1$ ) and the associated wave length are very close to the  $n = 0$  mode; the peak growth rate for  $n = 1$  modes exceeds  $n = 0$  when the viscosity of the liquid jet is large. The effects of viscosity on the irrotational instabilities are very strong. The analysis predicts that breakup fragments of liquids in high speed air streams may be exceedingly small, especially in the transonic range of Mach numbers.

*Keywords:* Capillary instability; Kelvin-Helmholtz instability; Isentropic compressible gas; Viscous potential flow; Irrotational flow of viscous fluids

## 1 Introduction

The problem of an inviscid liquid jet in an inviscid compressible airstream was studied by Chang & Russel (1965), Nayfeh & Saric (1973), Zhou & Lin (1992) and Li & Kelly (1992). Chawla (1975) studied the stability of a sonic gas jet submerged in a liquid. Chang & Russel (1965) and Nayfeh & Saric (1973) consider temporal instability and found that a singularity in the growth rate occurs as the Mach number tends to unity. Chawla (1975) did not find a singular growth rate but he restricted his attention to Mach number one ( $M = 1$ ). Li & Kelly (1992) found that the growth rates reach a sharp maximum when the gas velocity is slightly larger than the one giving  $M = 1$  for both axisymmetric and the first non-axisymmetric mode of instability. Lin (2003) cites Li & Kelly (1992) for the growth rate near  $M = 1$  in the case of temporal stability.

Here we extend the theory of viscous potential flow of a viscous compressible gas given by Joseph (2003) to the case of perturbations in a compressible gas moving with uniform velocity. We derive a dispersion relation for the perturbations which depend on all the material properties of the incompressible liquid and compressible gas. The effects of shear are neglected, consistent with the assumption that the basic flow can support a discontinuous velocity. We find a sharply peaking growth rate at slightly supersonic value of the gas Mach number under the conditions that Li & Kelly (1992) find steep changes for both axisymmetric and first asymmetric modes. The analysis of Li & Kelly (1992) differs from the one given here in the way that the isentropic flow is represented. They assume that  $dp/d\rho = c^2$ , as in isentropic flow, but they do not account for the usual isentropic relations which tie the density, pressure and velocity together as in our equation (4.3).

The first application of viscous potential flow to the problem of capillary instability was done by Funada & Joseph (2002). The problem of combined Kelvin-Helmholtz and capillary instability for an incompressible liquid and gas was done by Funada *et al.* (2004) who treated also the problem of convective and absolute instability in a comprehensive manner.

The effects of compressibility are very important for transonic and supersonic flow as has already been noted by Lin (2003). These effects include very great increases in growth rates and very sharp decreases in the wave length for maximum growth. This feature may possibly play a role in the breakup of liquid droplets into fine drops must observed in shock tube and wind tunnel experiments (Engel (1958), Joseph *et al.* (1999), Joseph *et al.* (2002), Theofanous *et al.* (2003), Varga *et al.* (2003)).

Chen & Li (1999) did a linear stability analysis for a viscous liquid jet issued into an inviscid moving compressible gas medium. Their analysis differs from ours; they do not assume that motion of the liquid is irrotational; they give results

---

<sup>‡</sup>Corresponding author: Tel.: +1-612-626-8000; fax: +1-612-626-1558. *E-mail address:* joseph@aem.umn.edu (D.D.Joseph).

only for the case in which the gas is at rest so that the effects of the basic flow gas velocity is not connected to the basic flow density and pressure as in the case of isotropic flow considered here. They do not compute growth rates for temporal instabilities for supersonic values  $M > 1$ . Their growth rate curves do not exhibit the same great increases in transonic and supersonic flow found by other authors and here.

The assumption that the gas is inviscid is not justified for jets of liquids into air especially when the air velocity is large. What matters here is the ratios of kinematic viscosities (see equation (4.2) in Funada *et al.* (2004) and figure 4 in Funada & Joseph (2001)) and the kinematic viscosity of high speed air in isentropic flow can be much greater than the kinematic viscosity of water.

Experimental results on liquid jets in high speed gas suitable for comparison with this and other analytical studies are not available. The coaxial jet experiments of Varga *et al.* (2003) discussed in section 12 is suitable, but they do not present data for transonic and supersonic conditions. Dunne & Cassen (Dunne & Cassen (1954), Dunne & Cassen (1956)) did some experiments on supersonic liquid jets. They injected high speed jets into air with a spring-loaded injector (1954) and by subjecting the liquid reservoir to a shock wave pressure (1956). These jets are transients and they appear to give rise to Rayleigh-Taylor instabilities on the front face of the jet as in the problem of drop breakup in high speed air and to Kelvin-Helmholtz wave at sides of the jets where the velocity is discontinuous. The data presented by them is not suitable for comparison on the analysis given here.

## 2 Basic partial differential equations

For isentropic compressible fluids, the equation of continuity, the viscous stress tensor  $\mathbf{T}$  and the equation of motion are expressed, in usual notation with the velocity potential  $\phi$  for which  $\mathbf{v} = \nabla\phi$  and  $\nabla \times \mathbf{v} = \mathbf{0}$ , as

$$\frac{\partial \rho}{\partial t} + \nabla \cdot (\rho \mathbf{v}) = 0, \quad \text{hence} \quad \frac{\partial \rho}{\partial t} + (\nabla \phi \cdot \nabla) \rho + \rho \nabla^2 \phi = 0, \quad (2.1)$$

$$T_{ij} = \mu \left( \frac{\partial v_i}{\partial x_j} + \frac{\partial v_j}{\partial x_i} \right) - \frac{2\mu}{3} (\nabla \cdot \mathbf{v}) \delta_{ij} = 2\mu \frac{\partial^2 \phi}{\partial x_i \partial x_j} - \frac{2\mu}{3} (\nabla^2 \phi) \delta_{ij}, \quad (2.2)$$

$$\frac{\partial \mathbf{v}}{\partial t} + (\mathbf{v} \cdot \nabla) \mathbf{v} = -\frac{1}{\rho} \nabla p + \frac{1}{\rho} \nabla \cdot \mathbf{T} \quad \rightarrow \quad \frac{\partial \phi}{\partial t} + \frac{1}{2} |\nabla \phi|^2 + \frac{\gamma}{\gamma - 1} \frac{p}{\rho} - \frac{4}{3} \frac{\mu}{\rho} \nabla^2 \phi = B(t). \quad (2.3)$$

The isentropic relation is given by

$$p \rho^{-\gamma} = \text{constant} \equiv A, \quad \text{hence} \quad p = A \rho^\gamma \quad (2.4)$$

with the adiabatic exponent  $\gamma$  and the sound velocity  $c$

$$c^2 = \frac{dp}{d\rho} = \gamma \frac{p}{\rho}. \quad (2.5)$$

These are used for viscous potential flow (VPF), which reduces to the inviscid potential flow (IPF) when the viscosity vanishes.

## 3 Cylindrical liquid jet in a compressible gas

A cylindrical liquid jet is surrounded by a compressible gas and is addressed in  $0 \leq r < a$  (where  $a$  is the radius of the cylindrical jet in an undisturbed state) and  $-\infty < z < \infty$  in the cylindrical frame  $(r, \theta, z)$ . The equation of continuity, the viscous stress tensor and Bernoulli function are given for the compressible gas

$$\left. \begin{aligned} \frac{\partial \rho_a}{\partial t} + (\nabla \phi_a \cdot \nabla) \rho_a + \rho_a \nabla^2 \phi_a &= 0, \\ T_{ij}^{(a)} &= 2\mu_a \frac{\partial^2 \phi_a}{\partial x_i \partial x_j} - \frac{2\mu_a}{3} (\nabla^2 \phi_a) \delta_{ij}, \\ \frac{\partial \phi_a}{\partial t} + \frac{1}{2} |\nabla \phi_a|^2 + \frac{\gamma}{\gamma - 1} \frac{p_a}{\rho_a} - \frac{4}{3} \frac{\mu_a}{\rho_a} \nabla^2 \phi_a &= B_a(t), \\ p_a = A \rho_a^\gamma \quad \rightarrow \quad \frac{dp_a}{d\rho_a} &= \gamma A \rho_a^{\gamma-1} = \gamma \frac{p_a}{\rho_a} = c_a^2, \end{aligned} \right\} \quad (3.1)$$

and for the liquid

$$\left. \begin{aligned} \rho_\ell = \text{constant}, \quad \nabla^2 \phi_\ell = 0, \quad T_{ij}^{(\ell)} = 2\mu_\ell \frac{\partial^2 \phi_\ell}{\partial x_i \partial x_j}, \\ \frac{\partial \phi_\ell}{\partial t} + \frac{1}{2} |\nabla \phi_\ell|^2 + \frac{p_\ell}{\rho_\ell} = B_\ell(t). \end{aligned} \right\} \quad (3.2)$$

Boundary conditions at the interface  $r = a + \eta$  (where  $\eta = \eta(\theta, z, t)$  is the interface displacement) are the kinematic conditions:

$$\frac{\partial \eta}{\partial t} + (\nabla \phi_a \cdot \nabla) \eta = \mathbf{n} \cdot \nabla \phi_a, \quad \frac{\partial \eta}{\partial t} + (\nabla \phi_\ell \cdot \nabla) \eta = \mathbf{n} \cdot \nabla \phi_\ell \quad (3.3)$$

with the outer normal vector  $\mathbf{n}$

$$\mathbf{n} = \left( 1, \frac{-1}{a + \eta} \frac{\partial \eta}{\partial \theta}, -\frac{\partial \eta}{\partial z} \right) / \sqrt{1 + \left( \frac{1}{a + \eta} \frac{\partial \eta}{\partial \theta} \right)^2 + \left( \frac{\partial \eta}{\partial z} \right)^2}, \quad (3.4)$$

and the normal stress balance:

$$p_\ell - p_a + \left( n_i T_{ij}^{(a)} n_j \right) - \left( n_i T_{ij}^{(\ell)} n_j \right) = \sigma \nabla \cdot \mathbf{n}, \quad (3.5)$$

where  $\sigma$  is the interfacial tension coefficient.

## 4 Basic isentropic relations

A basic state of the gas is with a uniform flow  $\bar{\mathbf{v}}_a = \nabla \bar{\phi}_a = (0, 0, U_a)$  in the frame  $(r, \theta, z)$  and with the constant density  $\rho_{a1}$  and pressure  $p_{a1}$ , and a basic state of the liquid is with a uniform flow  $\bar{\mathbf{v}}_\ell = \nabla \bar{\phi}_\ell = (0, 0, U_\ell)$  and with the constant density  $\rho_{\ell 1}$  and pressure  $p_{\ell 1}$ . The isentropic relation and the Bernoulli function lead for the gas to

$$\left. \begin{aligned} p_{a1} = A \rho_{a1}^\gamma = p_{a0} \left( \frac{\rho_{a1}}{\rho_{a0}} \right)^\gamma, \quad \frac{dp_{a1}}{d\rho_{a1}} = \gamma A \rho_{a1}^{\gamma-1} = \gamma \frac{p_{a1}}{\rho_{a1}} = c_a^2, \\ \frac{1}{2} U_a^2 + \frac{\gamma}{\gamma-1} \frac{p_{a1}}{\rho_{a1}} = \frac{1}{2} U_a^2 + \frac{c_a^2}{\gamma-1} = \frac{c_{a0}^2}{\gamma-1} = B_a, \quad \text{hence} \quad \left[ \frac{\gamma-1}{2} M_a^2 + 1 \right] \frac{\gamma p_{a1}}{\rho_{a1}} = \frac{\gamma p_{a0}}{\rho_{a0}}, \end{aligned} \right\} \quad (4.1)$$

where the Mach number  $M_a$  is defined as

$$M_a = \frac{U_a}{c_a}, \quad (4.2)$$

and  $\rho_{a0}$ ,  $p_{a0}$  and  $c_{a0}$  ( $c_{a0}^2 = \gamma p_{a0} / \rho_{a0}$ ) are defined when  $M_a = 0$ .

Using (4.1), we have

$$\left. \begin{aligned} \bar{\rho}_a = \frac{\rho_{a1}}{\rho_{a0}} = \left[ \frac{\gamma-1}{2} M_a^2 + 1 \right]^{-1/(\gamma-1)}, \quad \bar{p}_a = \frac{p_{a1}}{p_{a0}} = \left( \frac{\rho_{a1}}{\rho_{a0}} \right)^\gamma, \\ \frac{c_a^2}{c_{a0}^2} = \left[ \frac{\gamma-1}{2} M_a^2 + 1 \right]^{-1} \quad \text{or} \quad c_a^2 = c_{a0}^2 - \frac{\gamma-1}{2} U_a^2, \end{aligned} \right\} \quad (4.3)$$

in which the sound velocity  $c_a$  is given as a function of  $U_a$ . The thermodynamic properties of the ambient gas depend on the Mach number and the reference state when  $M_a = 0$ . For air of  $\rho_{a0} = 1.2 \text{ kg/m}^3$ ,  $p_{a0} = 1 \text{ atm} = 1.013 \times 10^5 \text{ Pa}$ ,  $c_{a0} = 340 \text{ m/sec}$ , and  $\gamma = 1.4$ . When  $M_a = 1$ , (4.3) gives  $c_a^2 = 2c_{a0}^2 / (\gamma + 1)$  for which  $c_a = 310.38 \text{ m/sec}$ . The third equation in (4.3) shows that  $c_a = 0 \text{ m/sec}$  when  $M_a \rightarrow \infty$ . Then  $U_a^2 = U_{am}^2 = 2c_{a0}^2 / (\gamma - 1)$  where  $U_{am} = 760.26 \text{ m/sec}$  is the maximum air velocity.

The Bernoulli function for the liquid leads to

$$\frac{1}{2} U_\ell^2 + \frac{p_{\ell 1}}{\rho_{\ell 1}} = B_\ell. \quad (4.4)$$

The kinematic conditions are satisfied for the unidirectional flows and the interface given by  $r = a$ . The normal stress balance is given by

$$p_{\ell 1} - p_{a1} = \frac{\sigma}{a}, \quad (4.5)$$

where  $\sigma/a$  denotes the capillary pressure.

## 5 Linear stability of the cylindrical liquid jet in a compressible gas; dispersion equation

On the basic flows, small disturbances are superimposed as

$$\left. \begin{aligned} \phi_\ell &= U_\ell z + \tilde{\phi}_\ell, \quad \rho_\ell = \rho_{\ell 1} \text{ (no perturbation)}, \quad p_\ell = p_{\ell 1} + \tilde{p}_\ell, \\ \phi_a &= U_a z + \tilde{\phi}_a, \quad \rho_a = \rho_{a1} + \tilde{\rho}_a, \quad p_a = p_{a1} + \tilde{p}_a. \end{aligned} \right\} \quad (5.1)$$

The isentropic relation gives

$$p_a = A\rho_a^\gamma, \quad \text{hence } p_{a1} = A\rho_{a1}^\gamma, \quad \tilde{p}_a \approx A\rho_{a1}^\gamma \gamma \frac{\tilde{\rho}_a}{\rho_{a1}} = c_a^2 \tilde{\rho}_a, \quad (5.2)$$

$$\frac{\gamma}{\gamma-1} \frac{p_a}{\rho_a} = \frac{c_a^2}{\gamma-1} + c_a^2 \frac{\tilde{\rho}_a}{\rho_{a1}} = \frac{c_a^2}{\gamma-1} + \frac{\tilde{p}_a}{\rho_{a1}}. \quad (5.3)$$

For the gas, we have the equations for the disturbance:

$$\left( \frac{\partial}{\partial t} + U_a \frac{\partial}{\partial z} \right) \tilde{\rho}_a + \rho_{a1} \nabla^2 \tilde{\phi}_a = 0, \quad \left( \frac{\partial}{\partial t} + U_a \frac{\partial}{\partial z} \right) \tilde{\phi}_a + c_a^2 \frac{\tilde{\rho}_a}{\rho_{a1}} - \frac{4}{3} \frac{\mu_a}{\rho_{a1}} \nabla^2 \tilde{\phi}_a = 0, \quad (5.4)$$

hence

$$\left( \frac{\partial}{\partial t} + U_a \frac{\partial}{\partial z} \right)^2 \tilde{\phi}_a = \left[ c_a^2 + \frac{4}{3} \frac{\mu_a}{\rho_{a1}} \left( \frac{\partial}{\partial t} + U_a \frac{\partial}{\partial z} \right) \right] \nabla^2 \tilde{\phi}_a. \quad (5.5)$$

For the liquid, we have the equations for the disturbance:

$$\nabla^2 \tilde{\phi}_\ell = 0, \quad \left( \frac{\partial}{\partial t} + U_\ell \frac{\partial}{\partial z} \right) \tilde{\phi}_\ell + \frac{\tilde{p}_\ell}{\rho_{\ell 1}} = 0. \quad (5.6)$$

At the interface  $r = a + \tilde{\eta} \approx a$  where  $\tilde{\eta} \equiv \tilde{\eta}(\theta, z, t)$  is the interface displacement, the kinematic conditions are given by

$$\frac{\partial \tilde{\eta}}{\partial t} + U_\ell \frac{\partial \tilde{\eta}}{\partial z} = \frac{\partial \tilde{\phi}_\ell}{\partial r}, \quad \frac{\partial \tilde{\eta}}{\partial t} + U_a \frac{\partial \tilde{\eta}}{\partial z} = \frac{\partial \tilde{\phi}_a}{\partial r}, \quad (5.7)$$

and the normal stress balance is given, on eliminating the pressures by using the Bernoulli functions, by

$$\begin{aligned} -\rho_{a1} \left( \frac{\partial}{\partial t} + U_a \frac{\partial}{\partial z} \right) \tilde{\phi}_a + 2\mu_a \left[ \nabla^2 \tilde{\phi}_a - \frac{\partial^2 \tilde{\phi}_a}{\partial r^2} \right] + \rho_{\ell 1} \left( \frac{\partial}{\partial t} + U_\ell \frac{\partial}{\partial z} \right) \tilde{\phi}_\ell + 2\mu_\ell \frac{\partial^2 \tilde{\phi}_\ell}{\partial r^2} \\ = \sigma \left( \frac{\partial^2 \tilde{\eta}}{\partial z^2} + \frac{1}{a^2} \frac{\partial^2 \tilde{\eta}}{\partial \theta^2} + \frac{\tilde{\eta}}{a^2} \right). \end{aligned} \quad (5.8)$$

The solution to the stability problem above formulated is expressed by normal modes

$$\left. \begin{aligned} \tilde{\phi}_\ell &= -i \frac{\omega - kU_\ell}{kI'_n(ka)} H I_n(kr) E + c.c., \quad \tilde{\phi}_a = -i \frac{\omega - kU_a}{\kappa K'_n(\kappa a)} H K_n(\kappa r) E + c.c., \\ \tilde{\eta} &= H E + c.c., \end{aligned} \right\} \quad (5.9)$$

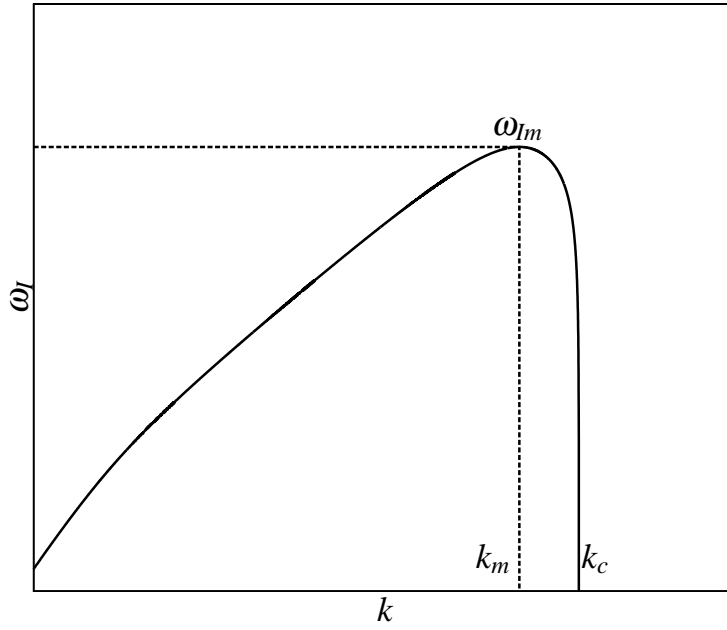


Figure 5.1: The form of a typical graph of the growth rate  $\omega_I$  versus  $k$ .  $\omega_{Im}$  is the maximum growth,  $\lambda_m = 2\pi/k_m$  is the wavelength of the fastest growing wave.  $k_c$  is the cut-off wavenumber.  $\omega_{Im}$  and  $k_m$  are called peak values.

where  $E \equiv \exp(ikz + in\theta - i\omega t)$  with the complex angular frequency  $\omega = \omega_R + i\omega_I$  and the real wavenumber  $k$ ,  $n$  denotes the azimuthal mode.  $I_n(kr)$  and  $K_n(\kappa r)$  are the modified Bessel functions, where the prime denotes the derivative  $I'_n(ka) = dI_n(ka)/d(ka)$ . The Bessel functions satisfy the equations

$$\left. \begin{aligned} \nabla^2 \tilde{\phi}_\ell &= \frac{\partial^2 \tilde{\phi}_\ell}{\partial r^2} + \frac{1}{r} \frac{\partial \tilde{\phi}_\ell}{\partial r} + \frac{1}{r^2} \frac{\partial^2 \tilde{\phi}_\ell}{\partial \theta^2} + \frac{\partial^2 \tilde{\phi}_\ell}{\partial z^2} = \frac{\partial^2 \tilde{\phi}_\ell}{\partial r^2} + \frac{1}{r} \frac{\partial \tilde{\phi}_\ell}{\partial r} - \frac{n^2}{r^2} \tilde{\phi}_\ell - k^2 \tilde{\phi}_\ell = 0, \\ \nabla^2 \tilde{\phi}_a - (\kappa^2 - k^2) \tilde{\phi}_a &= \frac{\partial^2 \tilde{\phi}_a}{\partial r^2} + \frac{1}{r} \frac{\partial \tilde{\phi}_a}{\partial r} - \frac{n^2}{r^2} \tilde{\phi}_a - \kappa^2 \tilde{\phi}_a = 0, \end{aligned} \right\} \quad (5.10)$$

with

$$\kappa = \sqrt{k^2 - \frac{(\omega - kU_a)^2}{c_a^2 - \frac{4i\mu_a}{3\rho_{a1}}(\omega - kU_a)}}, \quad (5.11)$$

which arise from (5.5) and (5.6). Substituting (5.9) into (5.7) and (5.8), we find the dispersion relation

$$\begin{aligned} & \left[ \rho_{a1} (\omega - kU_a)^2 - 2i\mu_a (\kappa^2 - k^2) (\omega - kU_a) \right] \frac{kK_n(\kappa a)}{\kappa K'_n(\kappa a)} - \rho_{\ell 1} (\omega - kU_\ell)^2 \frac{I_n(ka)}{I'_n(ka)} \\ & + 2i\mu_a k\kappa (\omega - kU_a) \frac{K''_n(\kappa a)}{K'_n(\kappa a)} - 2i\mu_\ell k^2 (\omega - kU_\ell) \frac{I''_n(ka)}{I'_n(ka)} + \sigma \left( k^2 - \frac{1-n^2}{a^2} \right) k = 0. \end{aligned} \quad (5.12)$$

The wave number  $k_m$  and maximum growth rate  $\omega_{Im}$  given by  $\omega_{Im} = \max \omega_I(k) = \omega_I(k_m)$  define the disturbance which is expected to appear in experiments. A typical dispersion relation is shown in figure 5.1. The cut-off wave number is the border of instability  $\omega_I(k_c) = 0$ .

## 6 Stability problem in dimensionless form

The scaling is made as

$$[\text{length, velocity, time}] = [d, c_a, d/c_a], \quad (6.1)$$

with  $d = 2a$ . The dimensionless variables are

$$(\hat{r}, \theta, \hat{z}) = \left( \frac{r}{d}, \theta, \frac{z}{d} \right), \quad \hat{t} = \frac{c_a}{d} t. \quad (6.2)$$

The hat on the independent variables are omitted for brevity. Then we may scale as

$$\left. \begin{aligned} \frac{\phi_\ell}{c_a d} &= \frac{U_\ell}{c_a} \hat{z} + \frac{\tilde{\phi}_\ell}{c_a d} = M_\ell \hat{z} + \hat{\phi}_\ell, & \frac{\rho_\ell}{\rho_{\ell 1}} &= 1, & \frac{p_\ell}{\rho_{\ell 1} c_a^2} &= \bar{p}_{\ell 1} + \frac{\tilde{p}_\ell}{\rho_{\ell 1} c_a^2} = \bar{p}_{\ell 1} + \hat{p}_\ell, \\ \frac{\phi_a}{c_a d} &= \frac{U_a}{c_a} \hat{z} + \frac{\tilde{\phi}_a}{c_a d} = M_a \hat{z} + \hat{\phi}_a, & \frac{\rho_a}{\rho_{a 1}} &= \frac{\rho_{a 1}}{\rho_{a 1}} + \frac{\tilde{\rho}_a}{\rho_{a 1}} = 1 + \hat{\rho}_a, & \hat{p}_a &= \frac{\tilde{p}_a}{\rho_{\ell 1} c_a^2} = \frac{\tilde{p}_a}{\rho_{\ell 1}} = \ell \hat{\rho}_a, \end{aligned} \right\} \quad (6.3)$$

where  $\bar{\phantom{x}}$  denotes the normalized basic flow and  $\hat{\phantom{x}}$  denotes the normalized disturbances, and the parameters are defined as

$$\ell = \frac{\rho_{a 1}}{\rho_{\ell 1}}, \quad m = \frac{\mu_a}{\mu_\ell}, \quad \nu = \frac{\mu_a \rho_{\ell 1}}{\mu_\ell \rho_{a 1}} = \frac{m}{\ell}, \quad M_\ell = \frac{U_\ell}{c_a}, \quad M_a = \frac{U_a}{c_a}, \quad R = \frac{\rho_{\ell 1} c_a d}{\mu_\ell}, \quad W = \frac{\sigma}{\rho_{\ell 1} d c_a^2}, \quad (6.4)$$

where the basic state of the gas is the function of the Mach number, with

$$\left. \begin{aligned} \frac{\rho_{a 1}}{\rho_{a 0}} &= Q(M_a)^{-1/(\gamma-1)} \quad \text{where } Q(M_a) \equiv \frac{\gamma-1}{2} M_a^2 + 1, \\ \ell &= \ell_0 Q(M_a)^{-1/(\gamma-1)}, \quad \ell_0 = \rho_{a 0} / \rho_{\ell 1}, \quad \frac{p_{a 1}}{p_{a 0}} = \left( \frac{\rho_{a 1}}{\rho_{a 0}} \right)^\gamma, \quad \frac{c_a^2}{c_{a 0}^2} = \frac{1}{Q(M_a)}, \\ R &= R_0 / Q(M_a), \quad R_0 = \frac{\rho_{\ell 1} c_{a 0} d}{\mu_\ell}, \quad W = W_0 Q(M_a), \quad W_0 = \frac{\sigma}{\rho_{\ell 1} d c_{a 0}^2}, \\ \frac{1}{2} M_\ell^2 + \bar{p}_{\ell 1} &= \text{constant}. \end{aligned} \right\} \quad (6.5)$$

For the gas,

$$\left( \frac{\partial}{\partial t} + M_a \frac{\partial}{\partial z} \right) \hat{\rho}_a + \nabla^2 \hat{\phi}_a = 0, \quad \ell \left( \frac{\partial}{\partial t} + M_a \frac{\partial}{\partial z} \right) \hat{\phi}_a + \hat{p}_a - \frac{4m}{3R} \nabla^2 \hat{\phi}_a = 0. \quad (6.6)$$

The combination leads to

$$\left( \frac{\partial}{\partial t} + M_a \frac{\partial}{\partial z} \right)^2 \hat{\phi}_a = \left[ 1 + \frac{4m}{3\ell R} \left( \frac{\partial}{\partial t} + M_a \frac{\partial}{\partial z} \right) \right] \nabla^2 \hat{\phi}_a. \quad (6.7)$$

For the liquid,

$$\nabla^2 \hat{\phi}_\ell = 0, \quad \left( \frac{\partial}{\partial t} + M_\ell \frac{\partial}{\partial z} \right) \hat{\phi}_\ell + \hat{p}_\ell = 0. \quad (6.8)$$

At the interface  $r = 1/2 + \hat{\eta} \approx 1/2$  where  $\hat{\eta} \equiv \hat{\eta}(\theta, z, t)$  is the interface displacement, the kinematic conditions are given by

$$\frac{\partial \hat{\eta}}{\partial t} + M_\ell \frac{\partial \hat{\eta}}{\partial z} = \frac{\partial \hat{\phi}_\ell}{\partial r}, \quad \frac{\partial \hat{\eta}}{\partial t} + M_a \frac{\partial \hat{\eta}}{\partial z} = \frac{\partial \hat{\phi}_a}{\partial r}, \quad (6.9)$$

and the normal stress balance is given by

$$-\ell \left( \frac{\partial}{\partial t} + M_a \frac{\partial}{\partial z} \right) \hat{\phi}_a + \frac{2m}{R} \left( \nabla^2 \hat{\phi}_a - \frac{\partial^2 \hat{\phi}_a}{\partial r^2} \right) + \left( \frac{\partial}{\partial t} + M_\ell \frac{\partial}{\partial z} \right) \hat{\phi}_\ell + \frac{2}{R} \frac{\partial^2 \hat{\phi}_\ell}{\partial r^2} = W \left( \frac{\partial^2 \hat{\eta}}{\partial z^2} + \frac{\partial^2 \hat{\eta}}{\partial \theta^2} + \hat{\eta} \right). \quad (6.10)$$

The solution to the stability problem above formulated is expressed as

$$\left. \begin{aligned} \hat{\phi}_\ell &= -i \frac{\omega - kM_\ell}{kI'_n(k/2)} \hat{H} I_n(kr) E + c.c., & \hat{\phi}_a &= -i \frac{\omega - kM_a}{\kappa K'_n(\kappa/2)} \hat{H} K_n(\kappa r) E + c.c., \\ \hat{\eta} &= \hat{H} E + c.c., \end{aligned} \right\} \quad (6.11)$$

where  $E \equiv \exp(ikz + in\theta - i\omega t)$  with the complex angular frequency  $\omega = \omega_R + i\omega_I$  and the real wavenumber  $k$ ,  $I_n(kr)$  and  $K_n(\kappa r)$  are the modified Bessel functions, the prime denotes the derivative:  $I'_n(k/2) = dI_n(k/2)/d(k/2)$ ,  $\kappa$  is defined as

$$\kappa = \sqrt{k^2 - \frac{\theta^2}{1 - \frac{4im}{\ell R}\theta}}, \quad (6.12)$$

where

$$\theta = \omega - kM_a, \quad \theta_\ell = \omega - kM_\ell. \quad (6.13)$$

Therefore the dispersion relation is expressed as

$$\left[ \ell\theta^2 - \frac{2im}{R} (\kappa^2 - k^2) \theta \right] \frac{k}{\kappa} \alpha_{an} + \theta_\ell^2 \alpha_n + \frac{2imk\kappa}{R} \theta \beta_{an} + \frac{2ik^2}{R} \theta_\ell \beta_n = W (k^2 + 4n^2 - 4) k, \quad (6.14)$$

with

$$\alpha_{\ell n} = \frac{I_n(k/2)}{I'_n(k/2)}, \quad \alpha_{an} = -\frac{K_n(\kappa/2)}{K'_n(\kappa/2)}, \quad \beta_{n\ell} = \frac{I''_n(k/2)}{I'_n(k/2)}, \quad \beta_{an} = -\frac{K''_n(\kappa/2)}{K'_n(\kappa/2)}, \quad (6.15)$$

and  $\ell = \ell_0 Q(M_a)^{-1/(\gamma-1)}$ ,  $R = R_0/Q(M_a)$ ,  $W = W_0 Q(M_a)$  defined under (6.5).

It is sometimes convenient to change the frame of the analysis to one moving with the liquid velocity  $U_\ell$ . In this frame the undisturbed liquid jet is at rest and the gas moves with velocity  $U_A = U_a - U_\ell$ . This is a Galilean change of frame in which the new coordinates are

$$z' = z + U_\ell t \quad (6.16)$$

and

$$E = \exp(ikz + in\theta - i\omega_R t + \omega_I t) = \exp(ikz' + in\theta - i\Omega_R t + \omega_I t) \quad (6.17)$$

where

$$\Omega_R = \omega_R + U_\ell k \quad (6.18)$$

in a new frequency. However, the density, pressure and sound speed of the gas are determined by the ambient conditions and gas velocity, as in (4.3), and these quantities do not change in a Galilean change of frame. For this reason, problems of stability of liquid jets in which  $U_a$  and  $U_\ell$  are given, as in the experiments of Varga *et al.* (2003) discussed in section 12, are not simplified by a Galilean change of frame. In the analysis given in sections 7-11 we put  $M_\ell = 0$  and  $M_a = M$ . This is the case of a static liquid cylinder in a moving gas.

In nearly all the computations to follow,  $\ell_0$ ,  $R_0$  and  $W_0$  are evaluated under standard conditions for air-water given in table 6.1. In section 11 we allow  $W_0$  to vary; this can be thought to be the effect of changing surface tension.

## 7 Inviscid potential flow (IPF)

The problem of an inviscid liquid jet moving in an inviscid compressible gas was considered by Li & Kelly (1992). The dispersion relation for this problem is (6.14) with  $R \rightarrow \infty$  and  $m/R = 0$ ,

$$\kappa = \sqrt{k^2 - (\omega - kM)^2}, \quad \ell (\omega - kM)^2 \frac{k}{\kappa} \alpha_{an} + \omega^2 \alpha_{\ell n} = W (k^2 + 4n^2 - 4) k, \quad (7.1)$$

Table 6.1: Properties of air-water.

Diameter of liquid jet, $d$	0.001 m
Air viscosity $\mu_a$	$1.8 \times 10^{-5}$ N.s/m <sup>2</sup>
Air density $\rho_{a0}$	1.2 kg/m <sup>3</sup>
Water density $\rho_{\ell 1}$	1000 kg/m <sup>3</sup>
Surface tension coefficient $\sigma$	0.075 N/m
Ratio of the specific heats $\gamma$ (air)	1.4

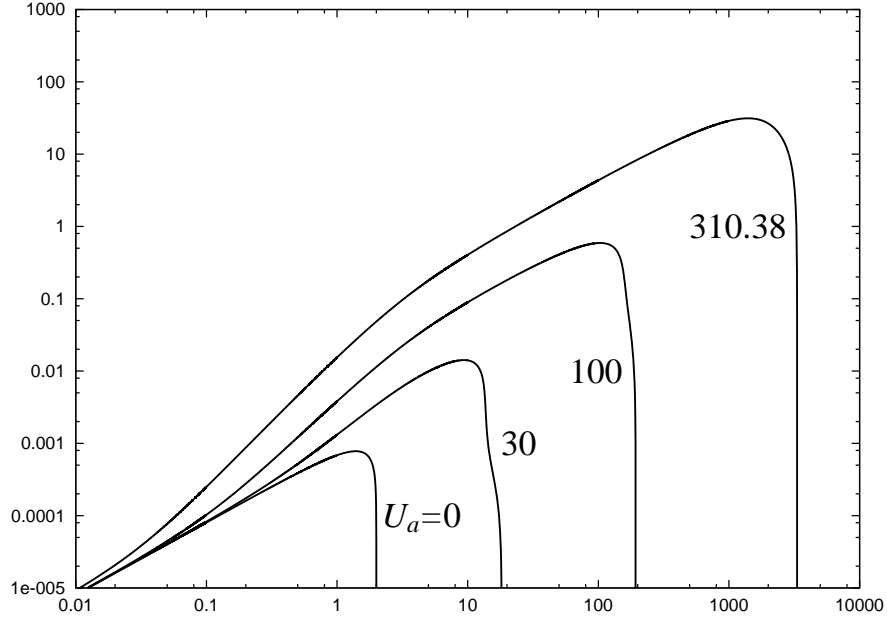


Figure 7.1: The growth rate  $\omega_I$  versus  $k$  in the axisymmetric  $n = 0$  mode for IPF, using the material parameters (table 6.1) for stationary water and air with  $U_a = 0, 30, 100$  and  $310.38$  m/sec. The values can be converted into dimensionless form  $(M, W)$  using table 8.1.

The parameters of this problem are  $\ell, n, M$  and  $W$ .

Pure capillary instability arises in the axisymmetric  $n = 0$  mode for large  $W$  and in the inviscid case is independent of the gas. The case  $W = 0$  is associated with pure Kelvin-Helmholtz instability for every  $n$  mode and it cannot occur in a vacuum ( $\ell \neq 0$ ). The variation of  $\omega_I$  versus  $k$  for an inviscid water in air is given in figure 7.1 with the  $n = 0$  mode.

The variation of growth rates with  $M$  for particular values of  $k, \sigma, U_a$  was given by Li & Kelly (1992); they did not present graphs of peak growth rates  $\omega_{Im}(k_m)$  and  $k_m$  as a function of  $M$ . At very high values of the Mach number

$$\ell = \ell_0/Q^{2.5} \rightarrow \ell_0/M^5 \quad (7.2)$$

and the first term of (7.1) may be neglective. Growth rate curves for IPF under standard condition and different Mach numbers are shown in figure 7.1.



## 8 Data for liquid jets with different viscosities in an airstream

In this section the data for stability computations is assembled in the tables 8.1 to 8.5. In table 8.1, we list the parameters for air under standard conditions and the liquid density, surface tension coefficient and the jet radius used in all the computations.

Table 8.2 to 8.5 list the data used in the stability computations and it lists the results of these computations. Each table gives results for one of four viscosities: 1, 300, 800 and 8000 cP. For each viscosity, computations were made for 27 values of  $U_a$  (table 8.1) and the results of 10 cases are shown in tables 8.2-8.5. Given  $\mu_\ell$ ,  $U_a$  and the data in table 8.1 the values of the material and dimensionless parameters are determined and listed in the columns of tables 8.2 to 8.5. Maximum value  $\omega_{Im}$  of the growth rate, the wave number  $k_m$  for  $\omega_{Im} = \omega_I(k_m)$  and the wave number  $k_c$  for which  $\omega_I(k_c) = 0$  (see figure 5.1 for a graphical representation of these values). Given  $(U_a, \mu_\ell)$  one may find values of  $M$ ,  $\ell$ ,  $W$  and  $R$  for a dimensionless representation.

Using the parameters of table 6.1, the viscosity ratio is evaluated as  $m = 1.8 \times 10^{-2}$  and the other basic nondimensional parameters which depends on  $U_a$  are shown in table 8.1. Negative values  $\omega_I < 0$  arise for non-axisymmetric  $n = 1$  disturbances when  $U_a$  is small. The entries in the columns  $n = 1$  in tables are left blanks.

Table 8.1: Typical values and nondimensional parameters for various  $U_a$  ( $U_\ell = 0$ ).

$U_a$ m/s	$c_a$	$p_{a1}$	$\rho_{a1}$	$\ell$	$M$	$R$	$W$
0.00	3.400e+02	1.013e+05	1.200e+0	1.200e-03	0.000e+0	3.400e+05	6.488e-07
0.10	3.400e+02	1.013e+05	1.200e+0	1.200e-03	2.941e-04	3.400e+05	6.488e-07
0.20	3.400e+02	1.013e+05	1.200e+0	1.200e-03	5.882e-04	3.400e+05	6.488e-07
0.50	3.400e+02	1.013e+05	1.200e+0	1.200e-03	1.471e-03	3.400e+05	6.488e-07
1.00	3.400e+02	1.013e+05	1.200e+0	1.200e-03	2.941e-03	3.400e+05	6.488e-07
5.00	3.400e+02	1.013e+05	1.200e+0	1.200e-03	1.471e-02	3.400e+05	6.488e-07
10.00	3.400e+02	1.012e+05	1.199e+0	1.199e-03	2.941e-02	3.400e+05	6.489e-07
20.00	3.399e+02	1.011e+05	1.198e+0	1.198e-03	5.884e-02	3.399e+05	6.492e-07
50.00	3.393e+02	9.977e+04	1.187e+0	1.187e-03	1.474e-01	3.393e+05	6.516e-07
70.00	3.386e+02	9.833e+04	1.175e+0	1.175e-03	2.068e-01	3.386e+05	6.543e-07
100.00	3.370e+02	9.530e+04	1.149e+0	1.149e-03	2.967e-01	3.370e+05	6.602e-07
150.00	3.333e+02	8.816e+04	1.087e+0	1.087e-03	4.500e-01	3.333e+05	6.751e-07
200.00	3.280e+02	7.881e+04	1.003e+0	1.003e-03	6.097e-01	3.280e+05	6.970e-07
250.00	3.211e+02	6.787e+04	9.014e-01	9.014e-04	7.786e-01	3.211e+05	7.274e-07
300.00	3.124e+02	5.602e+04	7.860e-01	7.860e-04	9.603e-01	3.124e+05	7.684e-07
310.38	3.104e+02	5.351e+04	7.607e-01	7.607e-04	1.000e+0	3.104e+05	7.786e-07
350.00	3.018e+02	4.401e+04	6.616e-01	6.616e-04	1.160e+0	3.018e+05	8.233e-07
400.00	2.891e+02	3.258e+04	5.337e-01	5.337e-04	1.383e+0	2.891e+05	8.971e-07
450.00	2.740e+02	2.239e+04	4.082e-01	4.082e-04	1.642e+0	2.740e+05	9.987e-07
500.00	2.561e+02	1.395e+04	2.911e-01	2.911e-04	1.952e+0	2.561e+05	1.143e-06
550.00	2.347e+02	7.573e+03	1.882e-01	1.882e-04	2.343e+0	2.347e+05	1.361e-06
600.00	2.088e+02	3.338e+03	1.048e-01	1.048e-04	2.873e+0	2.088e+05	1.720e-06
650.00	1.764e+02	1.023e+03	4.505e-02	4.505e-05	3.686e+0	1.764e+05	2.412e-06
700.00	1.327e+02	1.395e+02	1.085e-02	1.085e-05	5.276e+0	1.327e+05	4.261e-06
750.00	5.568e+01	3.199e-01	1.413e-04	1.413e-07	1.347e+01	5.568e+04	2.419e-05
760.00	8.944e+0	8.832e-07	1.512e-08	1.512e-11	8.497e+01	8.944e+03	9.375e-04
760.20	4.381e+0	5.973e-09	4.262e-10	4.262e-13	1.735e+02	4.381e+03	3.908e-03

Table 8.2: The table of peak values for  $\mu_\ell = 1$  cP in compressible gas.

$U_a$	$\mu_\ell = 1$ cP		$n = 0$			$n = 1$		
	$R$	$\nu$	$\omega_{Im}$	$k_m$	$k_c$	$\omega_{Im}$	$k_m$	$k_c$
0.00	3.400e+05	1.500e+01	7.790e-04	1.387e+00	1.999e+00	-	-	-
0.50	3.400e+05	1.500e+01	7.797e-04	1.396e+00	1.999e+00	1.228e-07	1.027e-02	2.341e-01
10.00	3.400e+05	1.501e+01	1.140e-03	1.891e+00	3.583e+00	2.218e-05	1.666e-01	2.962e+00
100.00	3.370e+05	1.567e+01	5.905e-01	1.027e+02	1.999e+02	5.902e-01	1.027e+02	1.999e+02
310.38	3.104e+05	2.366e+01	3.033e+01	1.432e+03	3.790e+03	3.033e+01	1.432e+03	3.790e+03
500.00	2.561e+05	6.183e+01	6.707e+00	9.919e+02	2.359e+03	6.707e+00	9.919e+02	2.359e+03
600.00	2.088e+05	1.717e+02	2.950e+00	8.317e+02	1.837e+03	2.950e+00	8.317e+02	1.837e+03
700.00	1.327e+05	1.658e+03	3.401e+00	1.153e+03	2.062e+03	3.401e+00	1.153e+03	2.062e+03
750.00	5.568e+04	1.274e+05	1.038e+01	1.315e+03	2.350e+03	1.038e+01	1.315e+03	2.350e+03
760.20	4.381e+03	4.224e+010	1.391e+02	1.351e+03	2.413e+03	1.391e+02	1.351e+03	2.413e+03

Table 8.3: The table of peak values for  $\mu_\ell = 300$  cP in compressible gas.

$U_a$	$\mu_\ell = 300$ cP		$n = 0$			$n = 1$		
	$R$	$\nu$	$\omega_{Im}$	$k_m$	$k_c$	$\omega_{Im}$	$k_m$	$k_c$
0.00	1.133e+03	5.000e-02	3.711e-04	9.325e-01	1.999e+00	-	-	-
0.50	1.133e+03	5.000e-02	3.713e-04	9.325e-01	1.999e+00	5.698e-08	1.000e-02	1.360e-02
10.00	1.133e+03	5.002e-02	4.635e-04	1.207e+00	2.683e+00	1.735e-05	5.815e-02	1.801e-01
100.00	1.123e+03	5.223e-02	4.801e-02	2.026e+01	1.585e+02	4.755e-02	2.089e+01	1.585e+02
310.38	1.035e+03	7.887e-02	1.515e+00	1.657e+02	1.522e+03	1.515e+00	1.657e+02	1.522e+03
500.00	8.537e+02	2.061e-01	9.396e-02	1.144e+01	4.645e+01	9.367e-02	1.126e+01	4.645e+01
600.00	6.960e+02	5.723e-01	3.802e-02	6.985e+00	2.341e+01	3.809e-02	6.391e+00	2.323e+01
700.00	4.422e+02	5.528e+00	4.186e-03	2.638e+00	6.148e+00	7.160e-03	1.252e+00	5.473e+00
750.00	1.856e+02	4.246e+02	2.437e-03	1.027e+00	2.233e+00	2.471e-03	3.916e-01	1.135e+00
760.20	1.460e+01	1.408e+08	2.910e-02	9.496e-01	2.053e+00	3.356e-02	3.970e-01	1.135e+00

Table 8.4: The table of peak values for  $\mu_\ell = 800$  cP in compressible gas.

$U_a$	$\mu_\ell = 800$ cP		$n = 0$			$n = 1$		
	$R$	$\nu$	$\omega_{Im}$	$k_m$	$k_c$	$\omega_{Im}$	$k_m$	$k_c$
0.00	4.250e+02	1.875e-02	2.006e-04	6.769e-01	1.999e+00	-	-	-
0.50	4.250e+02	1.875e-02	2.006e-04	6.778e-01	1.999e+00	-	-	-
10.00	4.250e+02	1.876e-02	2.324e-04	8.884e-01	2.683e+00	1.490e-05	3.943e-02	1.108e-01
100.00	4.213e+02	1.959e-02	1.972e-02	1.216e+01	1.585e+02	1.929e-02	1.360e+01	1.585e+02
310.38	3.880e+02	2.958e-02	7.069e-01	1.135e+02	1.522e+03	7.072e-01	1.144e+02	1.522e+03
500.00	3.202e+02	7.729e-02	3.912e-02	5.365e+00	2.845e+01	4.268e-02	3.997e+00	2.836e+01
600.00	2.610e+02	2.146e-01	1.451e-02	3.592e+00	1.432e+01	2.093e-02	1.747e+00	1.414e+01
700.00	1.658e+02	2.073e+00	1.264e-03	1.396e+00	4.402e+00	5.576e-03	5.752e-01	3.430e+00
750.00	6.960e+01	1.592e+02	1.277e-03	7.309e-01	2.179e+00	1.945e-03	2.251e-01	6.688e-01
760.20	5.476e+00	5.280e+07	1.561e-02	6.805e-01	2.008e+00	2.644e-02	2.368e-01	6.832e-01

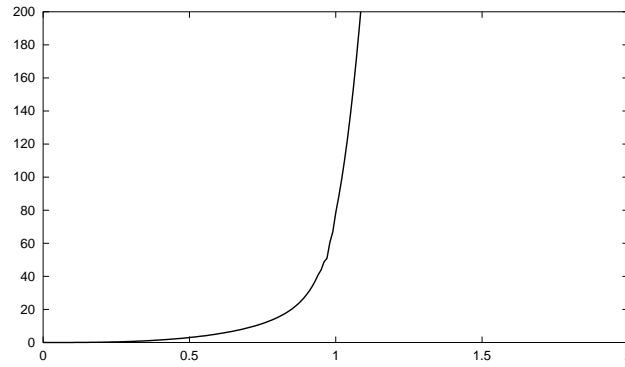
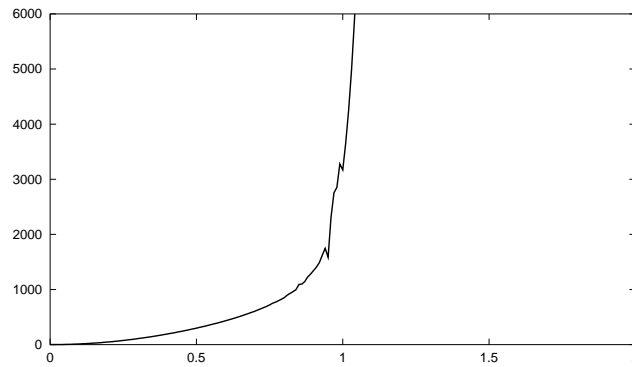
Table 8.5: The table of peak values for  $\mu_\ell = 8000$  cP in compressible gas.

$U_a$	$\mu_\ell = 8000$ cP		$n = 0$			$n = 1$		
	$R$	$\nu$	$\omega_{Im}$	$k_m$	$k_c$	$\omega_{Im}$	$k_m$	$k_c$
0.00	4.250e+01	1.875e-03	2.656e-05	2.431e-01	1.999e+00	-	-	-
0.50	4.250e+01	1.875e-03	2.656e-05	2.431e-01	1.999e+00	-	-	-
10.00	4.250e+01	1.876e-03	2.762e-05	4.177e-01	2.683e+00	8.636e-06	1.252e-02	3.556e-02
100.00	4.213e+01	1.959e-03	2.069e-03	8.065e+00	1.585e+02	2.219e-03	8.326e-01	1.585e+02
310.38	3.880e+01	2.958e-03	1.096e-01	5.104e+01	1.513e+03	1.094e-01	5.338e+01	1.513e+03
500.00	3.202e+01	7.729e-03	2.469e-03	1.828e+00	2.143e+01	1.646e-02	8.902e-01	1.981e+01
600.00	2.610e+01	2.146e-02	6.813e-04	1.387e+00	1.333e+01	9.624e-03	5.635e-01	1.234e+01
700.00	1.658e+01	2.073e-01	1.026e-04	6.481e-01	3.817e+00	2.388e-03	2.584e-01	2.386e+00
750.00	6.960e+00	1.592e+01	1.635e-04	2.692e-01	2.170e+00	1.025e-03	5.671e-02	1.990e-01
760.20	5.476e-01	5.280e+06	2.061e-03	2.431e-01	1.999e+00	1.348e-02	5.977e-02	2.161e-01

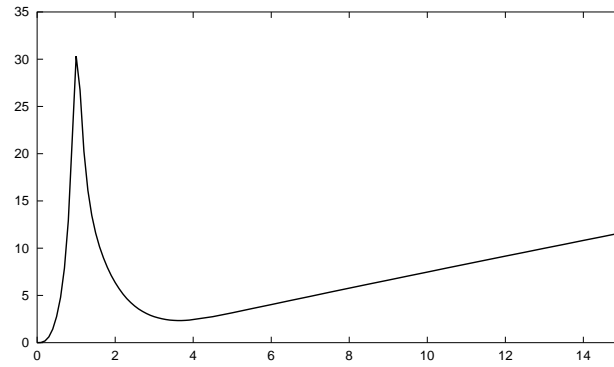
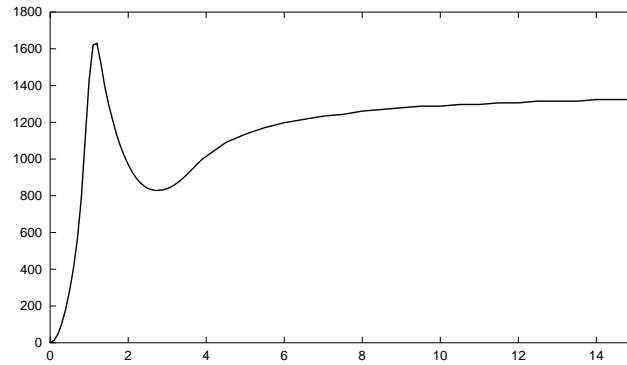
## 9 Variation of the maximum growth rate parameters with $M$ for different values of liquid viscosity

The variation of  $\omega_{Im}$  and  $k_m$  with  $M$  are displayed for  $\mu_\ell = 0, 1$  and  $300$  cP in figures 9.1 to 9.3. Results for  $\mu_\ell = 8000$  cP are displayed in 9.4; this is a low  $R$  case for which the mode with  $n = 1$  can be most dangerous. Otherwise  $\omega_{Im}$  and  $k_m$  for the modes with  $n = 0$  and  $n = 1$  are essentially the same.

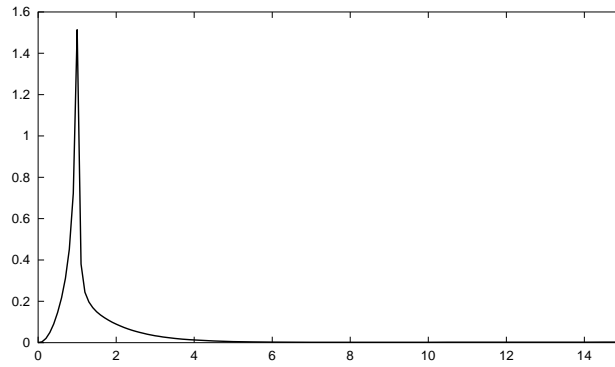
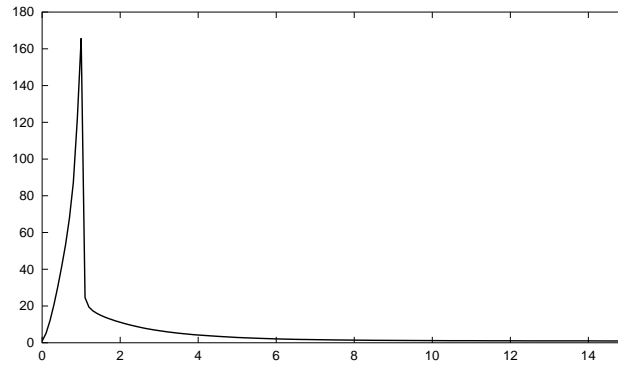
In figure 9.5 we blow up the sharply peaking growth rate curves  $\omega_I$  versus  $k$  for stationary liquid jets of small viscosity in high speed transonic air. The Mach numbers for the seven curves are [1, 2, 3, 4, 5, 6, 7]=[0.92, 0.96, 0.98, 1.01, 1.05, 1.08, 1.25] when  $\mu_\ell = 0.15$  cP and  $\mu_\ell = 0.175$  cP and for the nine curves [1, 2, 3, 4, 5, 6, 7, 8, 9]=[0.92, 0.96, 1.00, 1.05, 1.06, 1.12, 1.15, 1.20, 1.25] when  $\mu_\ell = 0.5$  cP.

(a) The maximum growth rate  $\omega_{Im}$  versus  $M$ .(b)  $k_m$  versus  $M$ .Figure 9.1: (a) The maximum growth rate  $\omega_{Im}$  versus  $M$ , (b)  $k_m$  versus  $M$  for IPF of  $n = 0$  in compressible gas.Table 9.1: Table of peak values of  $n = 0$  and  $n = 1$  for various  $M$ , IPF in compressible gas

$M$	$n = 0$			$n = 1$		
	$\omega_{Im}$	$k_m$	$k_c$	$\omega_{Im}$	$k_m$	$k_c$
0.00	7.821e-04	1.396e+00	2.008e+00	-	-	-
0.50	3.000e+00	2.989e+02	4.483e+02	3.000e+00	2.989e+02	4.483e+02
0.75	1.149e+01	7.192e+02	1.081e+03	1.149e+01	7.147e+02	1.081e+03
1.00	7.853e+01	3.169e+03	4.933e+03	7.853e+01	3.169e+03	4.933e+03
1.10	2.302e+02	1.540e+04	2.107e+04	2.302e+02	1.540e+04	2.107e+04
1.50	1.120e+03	2.656e+05	2.755e+05	1.120e+03	2.656e+05	2.755e+05
2.00	1.576e+03	8.560e+05	8.632e+05	1.576e+03	8.560e+05	8.632e+05

(a) The maximum growth rate  $\omega_{Im}$  versus  $M$ .(b)  $k_m$  versus  $M$ .Figure 9.2: (a) The maximum growth rate  $\omega_{Im}$  versus  $M$ , (b)  $k_m$  versus  $M$  for VPF ( $\mu_\ell = 1$  cP) of  $n = 0$  in compressible gas.Table 9.2: Table of peak values for various  $M$  (VPF:  $\mu_\ell = 1$  cP,  $m = 1.8 \times 10^{-2}$ )

$M$	$n = 0$			$n = 1$		
	$\omega_{Im}$	$k_m$	$k_c$	$\omega_{Im}$	$k_m$	$k_c$
0.00	7.790e-04	1.387e+00	2.008e+00	-	-	-
0.50	2.759e+00	2.845e+02	5.869e+02	2.759e+00	2.845e+02	5.869e+02
0.75	1.007e+01	6.670e+02	1.666e+03	1.007e+01	6.670e+02	1.666e+03
1.00	3.033e+01	1.432e+03	3.799e+03	3.033e+01	1.432e+03	3.799e+03
1.10	2.673e+01	1.621e+03	3.871e+03	2.673e+01	1.621e+03	3.871e+03
1.50	1.161e+01	1.297e+03	2.998e+03	1.161e+01	1.297e+03	2.998e+03
2.00	6.363e+00	9.703e+02	2.314e+03	6.363e+00	9.703e+02	2.314e+03

(a) The maximum growth rate  $\omega_{Im}$  versus  $M$ .(b)  $k_m$  versus  $M$ .Figure 9.3: (a) The maximum growth rate  $\omega_{Im}$  versus  $M$ , (b)  $k_m$  versus  $M$  for VPF ( $\mu_\ell = 300$  cP) of  $n = 0$  in compressible gas.Table 9.3: Table of peak values for various  $M$  (VPF:  $\mu_\ell = 300$  cP,  $m = 6 \times 10^{-5}$ )

$M$	$n = 0$			$n = 1$		
	$\omega_{Im}$	$k_m$	$k_c$	$\omega_{Im}$	$k_m$	$k_c$
0.00	3.711e-04	9.325e-01	2.008e+00	-	-	-
0.50	1.457e-01	4.123e+01	4.492e+02	1.453e-01	4.186e+01	4.492e+02
0.75	3.735e-01	7.651e+01	1.072e+03	3.731e-01	7.723e+01	1.072e+03
1.00	1.515e+00	1.657e+02	1.531e+03	1.515e+00	1.657e+02	1.531e+03
1.10	3.803e-01	2.458e+01	1.603e+02	3.897e-01	2.413e+01	1.603e+02
1.50	1.497e-01	1.495e+01	6.733e+01	1.501e-01	1.477e+01	6.733e+01
2.00	8.965e-02	1.117e+01	4.492e+01	8.934e-02	1.090e+01	4.483e+01

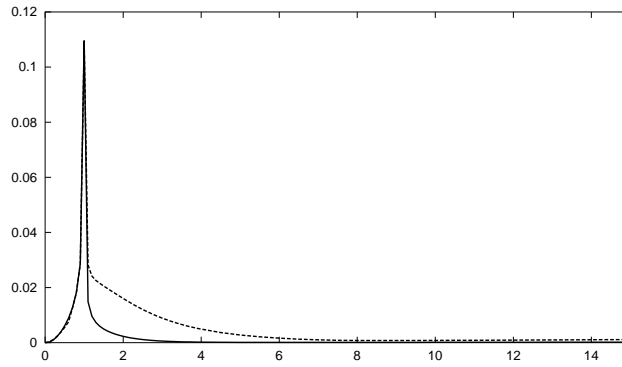
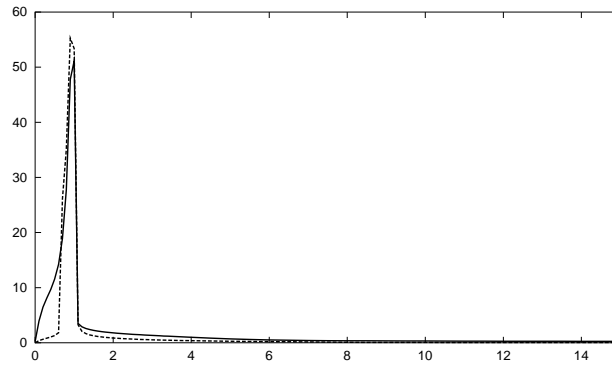
(a) The maximum growth rate  $\omega_{Im}$  versus  $M$ .(b)  $k_m$  versus  $M$ .

Figure 9.4: (a) The maximum growth rate  $\omega_{Im}$  versus  $M$ , (b)  $k_m$  versus  $M$ . VPF ( $\mu_\ell = 8000$  cP);  $n = 0$  in compressible gas (solid line) and  $n = 1$  in compressible gas (dashed line).

Table 9.4: Table of peak values for various  $M$  (VPF:  $\mu_\ell = 8000$  cP,  $m = 2.25 \times 10^{-6}$ )

$M$	$n = 0$			$n = 1$		
	$\omega_{Im}$	$k_m$	$k_c$	$\omega_{Im}$	$k_m$	$k_c$
0.00	2.656e-05	2.431e-01	2.008e+00	-	-	-
0.50	6.081e-03	1.153e+01	4.492e+02	5.959e-03	1.666e+01	4.492e+02
0.75	1.507e-02	2.260e+01	1.072e+03	1.494e-02	2.989e+01	1.072e+03
1.00	1.096e-01	5.113e+01	1.522e+03	1.095e-01	5.338e+01	1.522e+03
1.10	1.485e-02	3.511e+00	9.685e+01	2.818e-02	3.268e+00	9.712e+01
1.50	4.978e-03	2.251e+00	3.223e+01	2.056e-02	1.270e+00	2.989e+01
2.00	2.301e-03	1.801e+00	2.080e+01	1.604e-02	8.641e-01	1.927e+01



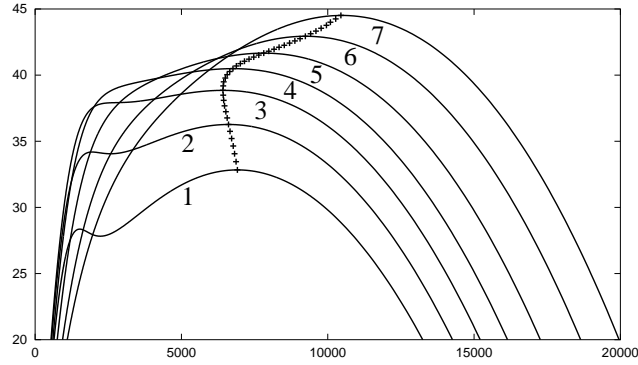
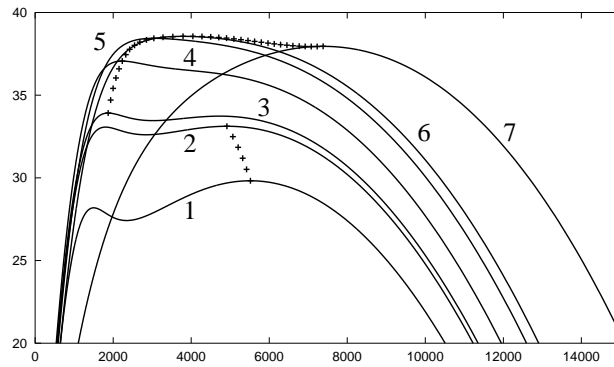
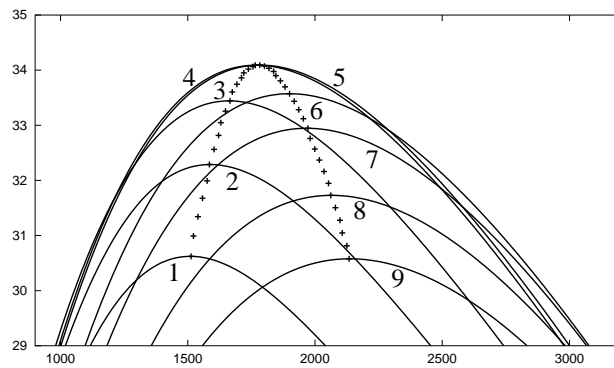
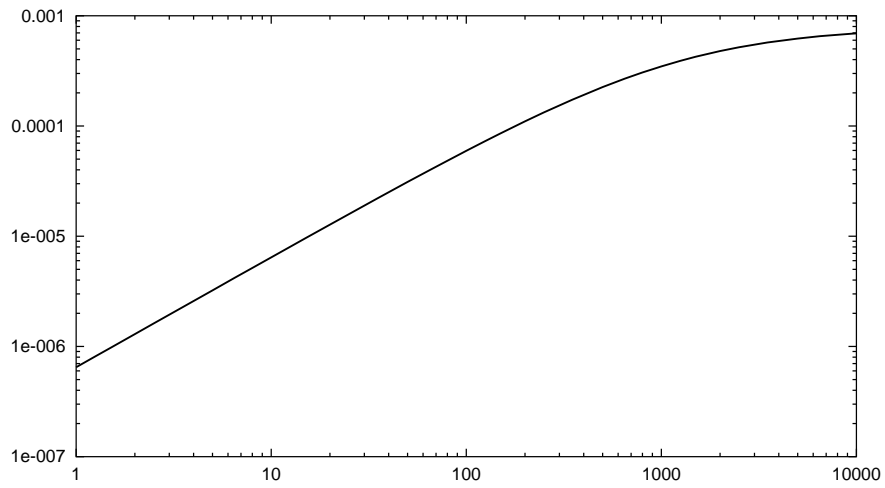
(a)  $\omega_I$  versus  $k$  for  $\mu_\ell = 0.15$  cP.(b)  $\omega_I$  versus  $k$  for  $\mu_\ell = 0.175$  cP.(c)  $\omega_I$  versus  $k$  for  $\mu_\ell = 0.5$  cP.

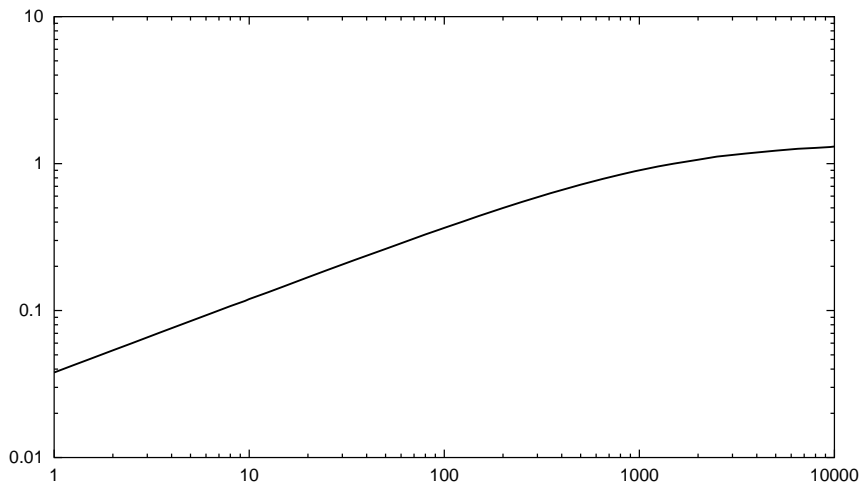
Figure 9.5: Growth rate versus wavenumber for stationary liquid jet ( $U_\ell = 0$ ) in transonic air.  $U_a = [1, 2, 3, 4, 5, 6, 7] = [290.08, 302.08, 314.08, 326.08, 340.08, 356.08, 370.08]$  m/s. (a)  $\mu_\ell = 0.15$  cP: as  $U_a$  increases, the maximum growth rate marked by + increases monotonically without limit. (b)  $\mu_\ell = 0.175$  cP: as  $U_a$  increases, the maximum growth rate marked by + increases, changes to another peak, attains the maximum near  $U_a = 310.38$  m/sec ( $M = 1$ ), and then decreases. (c)  $\mu_\ell = 0.5$  cP: as  $U_a$  increases, the maximum growth rate marked by + increases, attains the maximum near  $U_a = 310.38$  m/sec ( $M = 1$ ), and then decreases.

## 10 Azimuthal periodicity of the most dangerous disturbance

Batchelor & Gill (1962) argued that the conditions at the origin of a cylinder are such as to make the axisymmetric ( $n = 0$ ) mode and the  $n = 1$  mode of azimuthal periodicity most dangerous; all the modes except  $n = 1$  require that the radial and azimuthal components of the disturbance velocity vanish. The axial component of the disturbance velocity is single-valued only when  $n = 0$  (see Joseph (1976), pages 73, 74). Typical graphs showing the variation of these quantities with the Reynolds number for  $M = 0$ ,  $M = 0.5$  and  $M = 2$  are shown as figures (10.1, 10.2 and 10.3). Only the axisymmetric ( $n = 0$ ) mode gives rise to instability when  $M = 0$  (figure 10.1). Inspection of figures 10.2 and 10.3 show that the most dangerous mode is  $n = 1$  only for Reynolds numbers smaller than a number near 100; for larger Reynolds numbers the maximum growth rate and the most dangerous wave number are nearly the same for  $n = 0$  and  $n = 1$ .

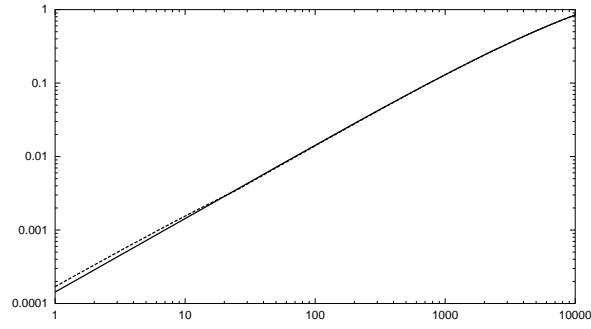


(a) The maximum growth rate  $\omega_{Im}$  versus  $R$  for  $M = 0$  and  $n = 0$ .

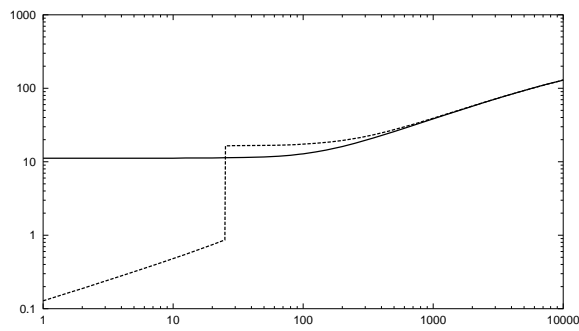


(b)  $k_m$  versus  $R$  for  $M = 0$  and  $n = 0$ .

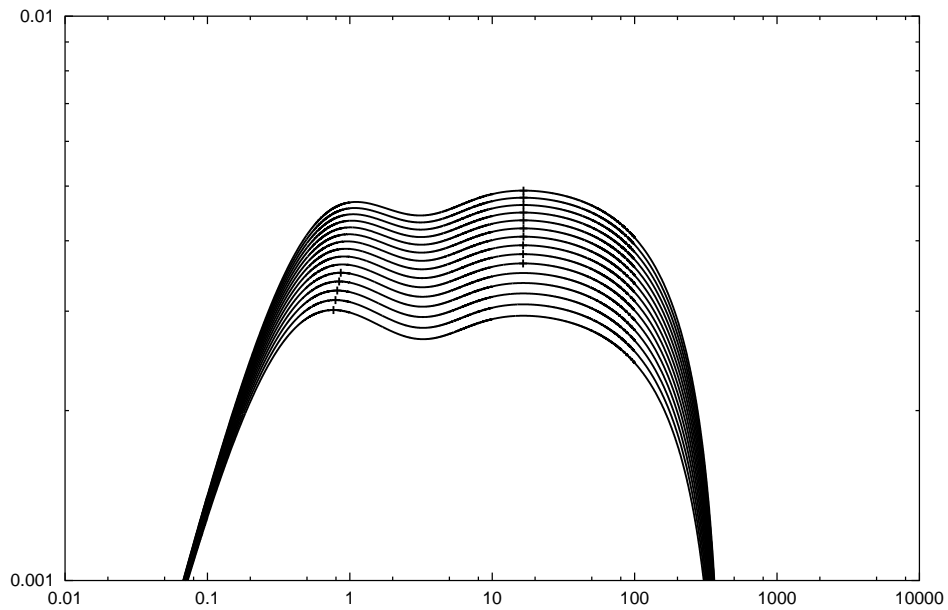
Figure 10.1: (a) the maximum growth rate  $\omega_{Im}$  versus  $R$ , (b)  $k_m$  versus  $R$ , for  $M = 0$  and  $n = 0$  in compressible gas. It is noted for  $M = 0$  that the capillary instability may arise only for  $n = 0$ , but K-H instability does not arise yet.



(a) The maximum growth rate  $\omega_{Im}$  versus  $R$ .



(b)  $k_m$  versus  $R$ . The growth rate curve  $\omega_I$  vs.  $k$  which is shown in figure 10.2 (c) has two relative maxima ; the absolute maxima changes for  $R_0$  between 25 and 26; this is seen as a jump in  $k$  in 10.2 (b).



(c)  $\omega_I$  vs.  $k$ .

Figure 10.2: (a) The maximum growth rate  $\omega_{Im}$  versus  $R$  and (b)  $k_m$  versus  $R$ , for  $M = 0.5$ ;  $n = 0$  in compressible gas (solid line) and  $n = 1$  in compressible gas (dashed line).

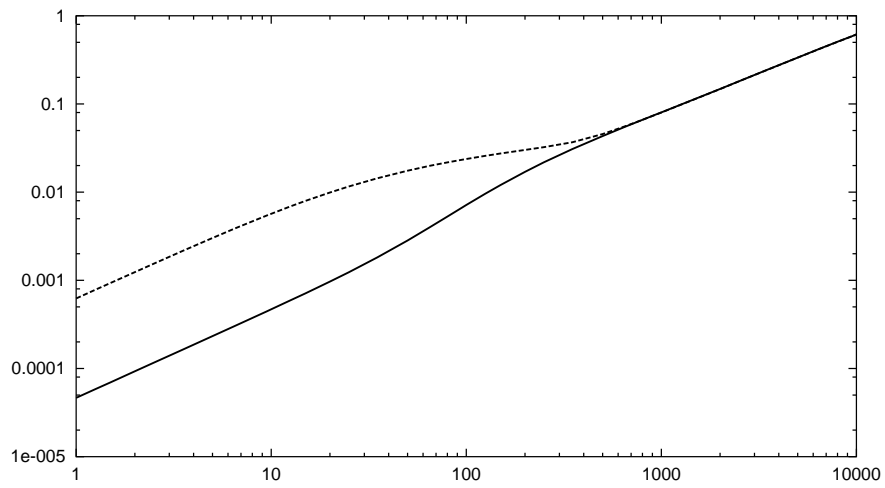
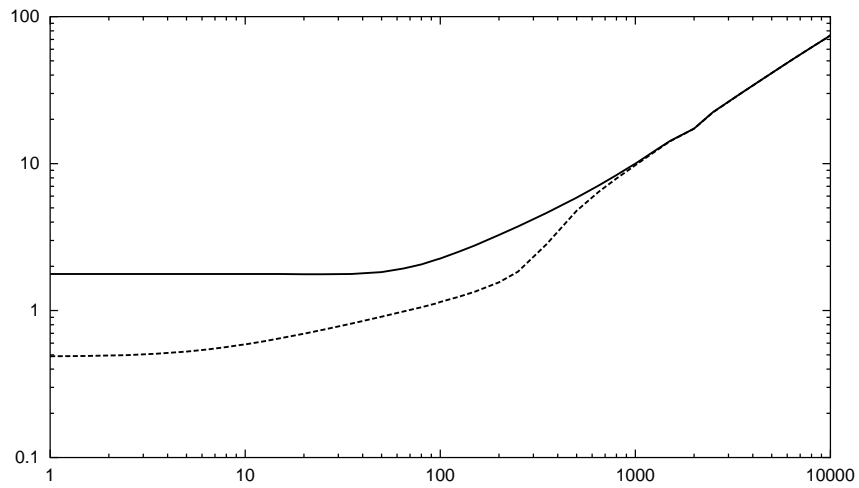
(a) The maximum growth rate  $\omega_{Im}$  versus  $R$ .(b)  $k_m$  versus  $R$ .

Figure 10.3: (a) The maximum growth rate  $\omega_{Im}$  versus  $R$  and (b)  $k_m$  versus  $R$ , for  $M = 2$ ;  $n = 0$  in compressible gas (solid line) and  $n = 1$  in compressible gas (dashed line).

## 11 Variation of the growth rate parameters with the Weber number

Graphs of  $\omega_{Im}$  and  $k_m$  versus  $W^{-1}$  are displayed for typical cases in figure 11.1, 11.2, 11.3 and 11.4. When  $W$  is large, the instability is dominated by capillarity; when  $W$  is small Kelvin-Helmholtz instability dominates. This behavior is characteristic also for the liquid jet in an incompressible gas which was studied by Funada *et al.* (2004); they used  $W^{-1}$  rather than  $W$  following earlier literature.

We have shown in section 9 that the most dangerous mode is typically axisymmetric when the Reynolds number is larger than about 100 as is true for the cases considered here. The graphs are all similar; for small values of  $W^{-1}$  in which capillarity dominates the values of  $\log \omega_{Im}$  decrease linearly with  $\log W^{-1}$  giving rise to a power law  $\omega_{Im} = a (W^{-1})^p$  where  $a$  and  $p$  may be determined from the graphs. The most dangerous wave number  $k_m = 1.396$  is a universal value which maximizes  $\omega_I$  when surface tension dominates. All the growth rate curves have a minimum value which marks the place where Kelvin-Helmholtz instability starts to be important, after this minimum  $\omega_{Im}$  and  $k_m$  increase with  $W^{-1}$ . In all case  $k_m \rightarrow \infty$  as  $W^{-1} \rightarrow \infty$ , but  $\omega_{Im}$  is lowered as  $W^{-1} \rightarrow \infty$  when the liquid viscosity is not zero.

Table 11.1: IPF,  $M = 0.5$ 

$W^{-1}$	$n = 0$			$n = 1$		
	$\omega_{Im}$	$k_m$	$k_c$	$\omega_{Im}$	$k_m$	$k_c$
1.00e-01	3.071e+00	1.396e+00	-	-	-	-
1.00e+00	9.710e-01	1.396e+00	-	-	-	-
1.00e+01	3.072e-01	1.396e+00	-	-	-	-
1.00e+02	9.770e-02	1.405e+00	-	-	-	-
1.00e+03	3.272e-02	1.468e+00	-	-	-	-
1.00e+04	2.062e-02	2.485e+00	-	4.306e-03	8.614e-01	-
1.00e+05	1.865e-01	2.008e+01	2.656e+01	1.833e-01	1.990e+01	2.539e+01
1.00e+06	2.037e+00	2.035e+02	-	2.037e+00	2.035e+02	2.710e+02

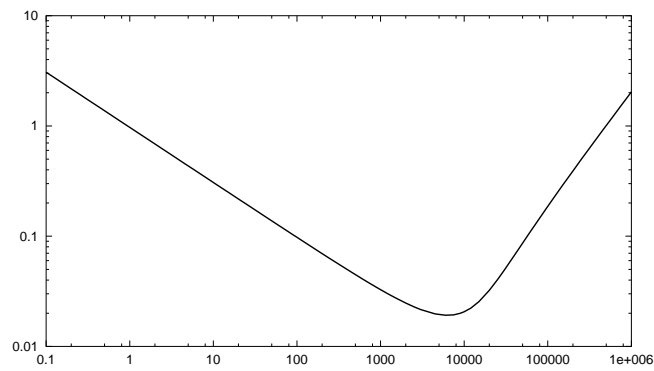
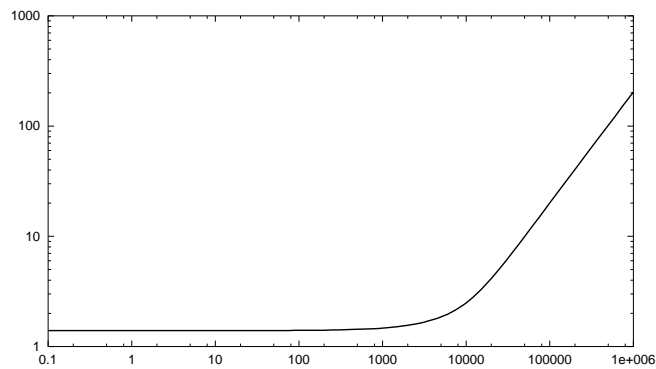
(a) The maximum growth rate  $\hat{\omega}_{Im}$  versus  $W^{-1}$ .(b)  $k_m$  versus  $W^{-1}$ .Figure 11.1: (a) The maximum growth rate  $\hat{\omega}_{Im}$  versus  $W^{-1}$ , (b)  $k_m$  versus  $W^{-1}$ ; IPF,  $M = 0.5$  for  $n = 0$  in compressible gas.

Table 11.2: VPF,  $M = 0.5$  for  $\mu_\ell = 1$  cP

$W^{-1}$	$n = 0$			$n = 1$		
	$\omega_{Im}$	$k_m$	$k_c$	$\omega_{Im}$	$k_m$	$k_c$
1.00e-01	3.071e+00	1.396e+00	1.999e+00	-	-	-
1.00e+00	9.710e-01	1.396e+00	1.999e+00	-	-	-
1.00e+01	3.072e-01	1.396e+00	1.999e+00	5.123e-08	3.862e-04	1.495e-01
1.00e+02	9.769e-02	1.405e+00	2.026e+00	1.109e-06	2.251e-03	6.967e-01
1.00e+03	3.272e-02	1.468e+00	2.287e+00	4.767e-06	9.766e-03	1.504e+00
1.00e+04	2.061e-02	2.485e+00	5.338e+00	4.304e-03	8.605e-01	4.618e+00
1.00e+05	1.854e-01	1.999e+01	4.024e+01	1.822e-01	1.990e+01	4.015e+01
1.00e+06	1.921e+00	1.963e+02	3.988e+02	1.921e+00	1.963e+02	3.988e+02

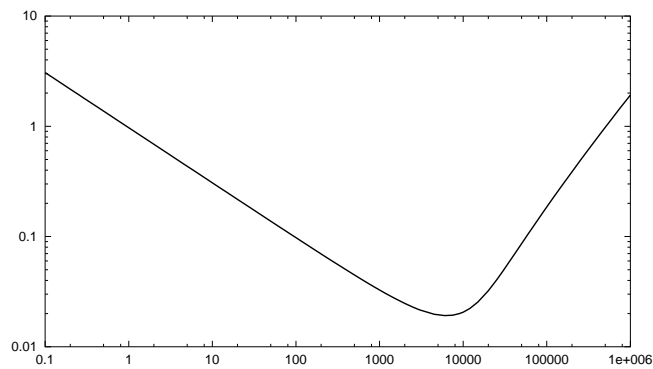
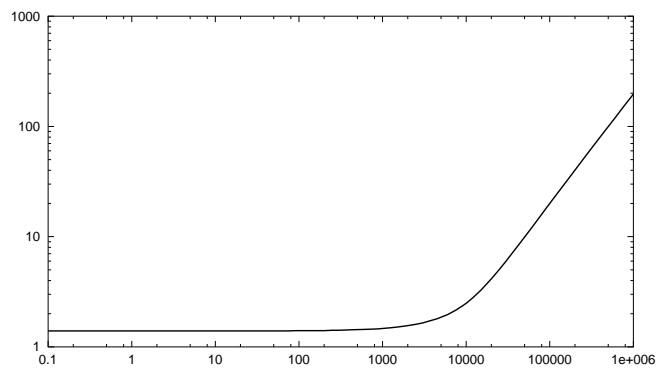
(a) The maximum growth rate  $\omega_{Im}$  versus  $W^{-1}$ .(b)  $k_m$  versus  $W^{-1}$ .Figure 11.2: (a) The maximum growth rate  $\omega_{Im}$  versus  $W^{-1}$ , (b)  $k_m$  versus  $W^{-1}$ , VPF,  $M = 0.5$  for  $\mu_\ell = 1$  cP, for  $n = 0$  in compressible gas.



Table 11.3: VPF,  $M = 0.5$  for  $\mu_\ell = 300$  cP

$W^{-1}$	$n = 0$			$n = 1$		
	$\omega_{Im}$	$k_m$	$k_c$	$\omega_{Im}$	$k_m$	$k_c$
1.00e-01	3.070e+00	1.396e+00	1.999e+00	-	-	-
1.00e+00	9.701e-01	1.396e+00	1.999e+00	-	-	-
1.00e+01	3.063e-01	1.396e+00	1.999e+00	-	-	8.686e-03
1.00e+02	9.677e-02	1.396e+00	2.008e+00	1.108e-06	6.931e-04	4.033e-02
1.00e+03	3.172e-02	1.450e+00	2.107e+00	4.758e-06	2.755e-03	8.326e-02
1.00e+04	1.784e-02	2.314e+00	3.502e+00	3.862e-03	8.011e-01	1.288e+00
1.00e+05	7.341e-02	1.126e+01	2.962e+01	7.055e-02	1.126e+01	2.944e+01
1.00e+06	1.396e-01	3.538e+01	3.052e+02	1.391e-01	3.583e+01	3.052e+02

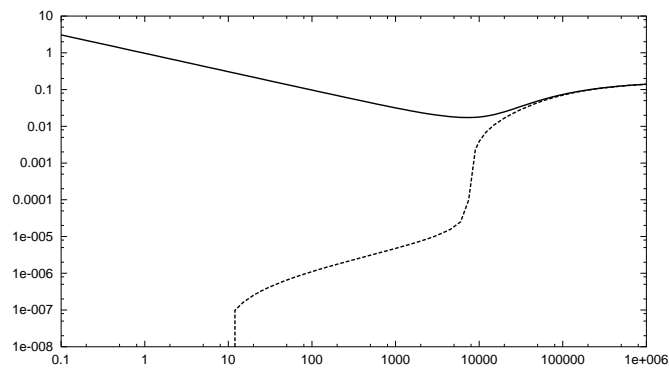
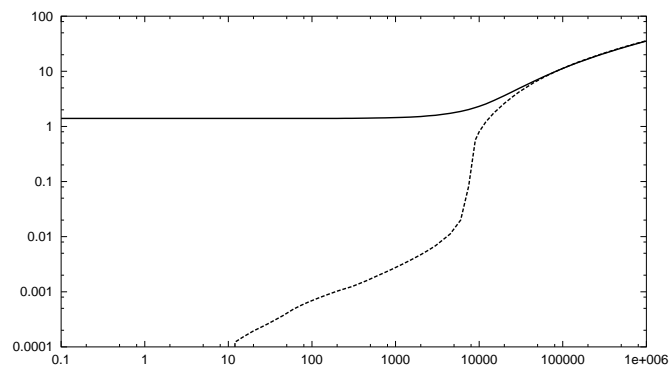
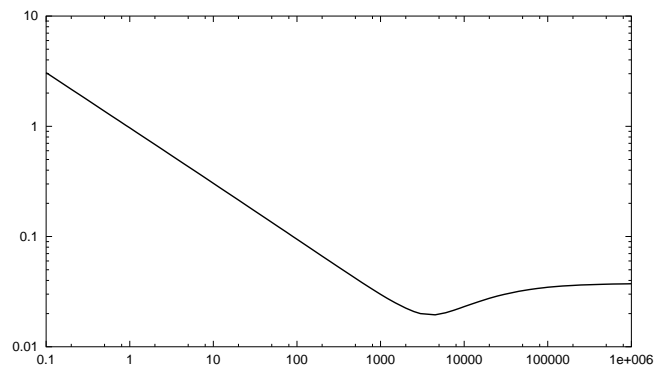
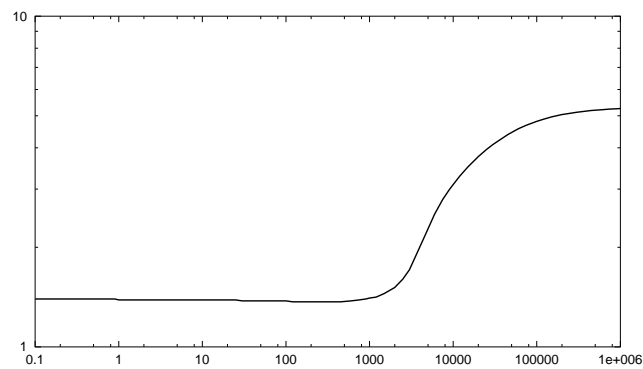
(a) The maximum growth rate  $\omega_{Im}$  versus  $W^{-1}$ .(b)  $k_m$  versus  $W^{-1}$ .Figure 11.3: (a) The maximum growth rate  $\omega_{Im}$  versus  $W^{-1}$ , (b)  $k_m$  versus  $W^{-1}$ . VPF,  $M = 0.5$  for  $\mu_\ell = 300$  cP;  $n = 0$  in compressible gas (solid line) and  $n = 1$  in compressible gas (dashed line).

Table 11.4: VPF,  $M = 2$  for  $\mu_\ell = 800$  cP

$W^{-1}$	$n = 0$			$n = 1$		
	$\omega_{Im}$	$k_m$	$k_c$	$\omega_{Im}$	$k_m$	$k_c$
1.00e-01	3.068e+00	1.396e+00	1.999e+00	-	-	-
1.00e+00	9.679e-01	1.387e+00	1.999e+00	-	-	9.964e-03
1.00e+01	3.040e-01	1.387e+00	1.999e+00	-	-	2.890e-02
1.00e+02	9.455e-02	1.378e+00	2.017e+00	-	-	5.959e-02
1.00e+03	2.992e-02	1.405e+00	2.224e+00	-	-	-
1.00e+04	2.312e-02	3.097e+00	5.203e+00	3.096e-02	1.819e+00	4.078e+00
1.00e+05	3.464e-02	4.807e+00	1.207e+01	3.919e-02	3.367e+00	1.189e+01
1.00e+06	3.728e-02	5.257e+00	2.935e+01	4.094e-02	3.844e+00	2.926e+01

(a) The maximum growth rate  $\omega_{Im}$  versus  $W^{-1}$ .(b)  $k_m$  versus  $W^{-1}$ .Figure 11.4: (a) The maximum growth rate  $\omega_{Im}$  versus  $W^{-1}$ , (b)  $k_m$  versus  $W^{-1}$ , VPF,  $M = 2$  for  $\mu_\ell = 800$  cP, for  $n = 0$  in compressible gas.

## 12 Coaxial jets

The problem of a liquid jet in a compressible gas flow is encountered in atomization experiments in coaxial jets discussed by Varga *et al.* (2003). They observed that the jet undulates due to Kelvin-Helmholtz instability and in the undulated configuration is at an angle to the air. The air stream then has a component normal to the KH waves giving rise to a secondary Rayleigh-Taylor instability which they claim is the primary cause of breakup. The analysis of this secondary instability is beyond the scope of our linear theory.

Varga *et al.* (2003) gave experimental results for jets of water and ethanol of different diameter and various jet speeds  $U_\ell$  and air speeds ranging flow 40 to 165 m/s. The air speeds are subsonic and even at the highest air speed (165 m/s) the effects of compressibility are modest. We carried out calculations for some of their experiments with data summarized in table 12.1. The growth rate curves in all these cases are like that shown in figure 5.1 so that it will suffice to present the results in the forms of tables of maximum growth rate parameters. In all cases, the growth rates are larger for the axisymmetric mode  $n = 0$  than for the mode with  $n = 1$ . However the maximum growth rates for  $n = 1$  are not much smaller so that mixture of these modes might be expected to occur in experiments. Mixed modes are existent in the experiments of Varga *et al.* (2003).

In figures 12.1 and 12.2 we present graphs of  $\omega_{Im}$ ,  $k_m$  and  $k_c$  versus  $U_\ell$  for coaxial jets of liquid into air studied by Varga *et al.* (2003) when  $U_a = 40$  m/sec under conditions listed in the table below. In figure 12.3 the same data is given for  $U_a = 165$  m/sec and in 12.4 for  $U_a = 265$  m/sec.

Table 12.1: (Varga *et al.* (2003)) Fluid properties.

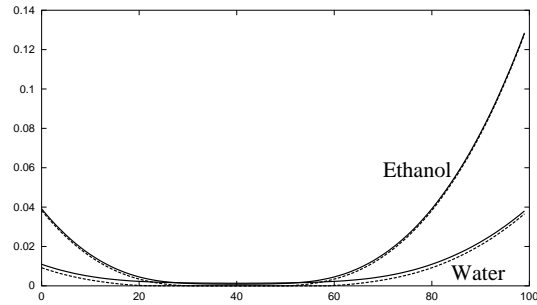
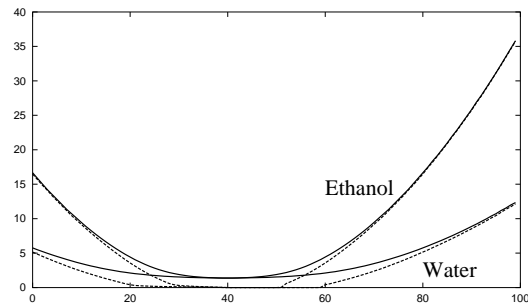
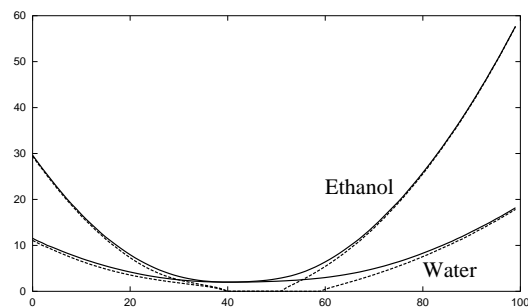
fluid	Density(kg m <sup>-3</sup> )	Viscosity(Pa s)	Surface tension(N/m)
Air	1.2	$1.8 \times 10^{-5}$	-
Water	998	$1.0 \times 10^{-3}$	0.070
Ethanol	791	$1.2 \times 10^{-3}$	0.023

Table 12.2:  $\omega_{Im}$ ,  $k_m$  and  $k_c$  for  $U_a = 40$  m/sec  $U_\ell = 60, 160, 260, 360, 460, 560, 660, 760$  m/sec. (1) water  $n = 0$ , (2) water  $n = 1$ , (3) ethanol  $n = 0$  and (4) ethanol  $n = 1$ .

		Compressible gas		
	$U_\ell$	$\omega_{Im}$	$k_m$	$k_c$
(1)	60	2.067e-01	3.601e+01	6.904e+01
	160	1.396e-03	1.423e+00	2.116e+00
	260	1.500e-01	2.926e+01	4.321e+01
	360	1.647e+00	1.414e+02	2.053e+02
	460	1.106e+01	4.888e+02	1.018e+03
	560	1.347e+01	7.597e+02	1.585e+03
	660	1.200e+01	7.444e+02	1.567e+03
	760	1.226e+01	7.408e+02	1.567e+03
(2)	60	2.057e-01	3.601e+01	6.895e+01
	160	9.133e-06	6.310e-02	1.144e+00
	260	1.489e-01	2.917e+01	4.312e+01
	360	1.647e+00	1.414e+02	2.053e+02
	460	1.106e+01	4.888e+02	1.018e+03
	560	1.347e+01	7.597e+02	1.585e+03
	660	1.200e+01	7.444e+02	1.567e+03
	760	1.226e+01	7.408e+02	1.567e+03
(3)	60	6.305e-01	1.009e+02	1.900e+02
	160	9.394e-04	1.477e+00	2.260e+00
	260	4.663e-01	8.236e+01	1.387e+02
	360	4.354e+00	3.610e+02	7.201e+02
	460	2.093e+01	8.866e+02	1.810e+03
	560	2.076e+01	9.910e+02	1.954e+03
	660	1.724e+01	8.947e+02	1.783e+03
	760	1.674e+01	8.461e+02	1.693e+03
(4)	60	6.302e-01	1.009e+02	1.900e+02
	160	2.000e-05	1.252e-01	1.387e+00
	260	4.658e-01	8.236e+01	1.387e+02
	360	4.353e+00	3.610e+02	7.201e+02
	460	2.092e+01	8.866e+02	1.810e+03
	560	2.076e+01	9.910e+02	1.954e+03
	660	1.724e+01	8.947e+02	1.783e+03
	760	1.674e+01	8.461e+02	1.693e+03

Table 12.3: Parameters for  $U_a = 40$  m/s.

fluid	$U_a$ (m/sec)	$D_\ell$ (m)	$M_a$	$W_e$	$R_e$	$m$	$\ell$
Water	4.000e+01	3.200e-04	1.178e-01	1.901e-06	1.084e+05	1.800e-02	1.194e-03
Ethanol	4.000e+01	3.200e-04	1.178e-01	7.882e-07	7.162e+04	1.500e-02	1.507e-03

(a) The maximum growth rate  $\omega_{Im}$  versus  $U_\ell$ .(b) The maximum growth rate  $\omega_{Im}$  versus  $U_\ell$ .(c) The cut off wave number  $k_c$  versus  $U_\ell$ .Figure 12.1: KH instability of liquid jet with  $U_\ell$  in compressible gas of  $U_a = 40$  m/s for  $0 < U_\ell < 100$  m/sec.  $n = 0$  solid lines,  $n = 1$  dashed lines.

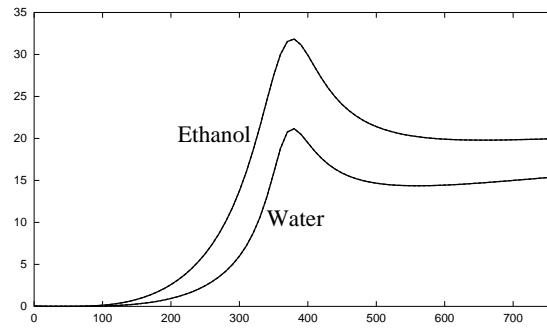
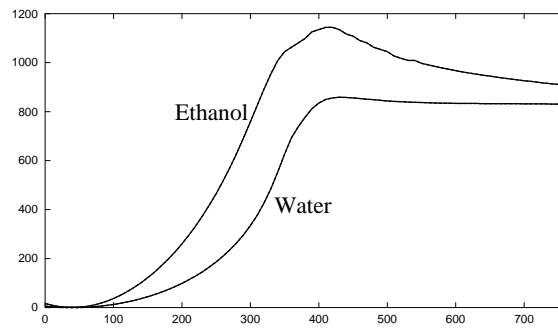
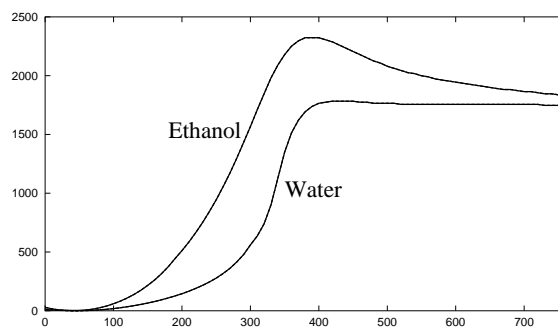
(a) The maximum growth rate  $\omega_{Im}$  versus  $U_\ell$ .(b) The maximum growth rate  $\omega_{Im}$  versus  $U_\ell$ .(c) The cut off wave number  $k_c$  versus  $U_\ell$ .

Figure 12.2: KH instability of liquid jet with  $U_\ell$  in compressible gas of  $U_a = 40$  m/s for  $0 < U_\ell < 800$  m/sec.  $n = 0$  solid lines. The graphs for  $n = 1$  coincide with  $n = 0$  for large values of  $U_\ell$ .

Table 12.4: Parameters for  $U_a = 165$  m/s.

fluid	$U_a$ (m/sec)	$D_\ell$ (m)	$M_a$	$W_e$	$R_e$	$m$	$\ell$
Water	1.650e+02	3.200e-04	4.971e-01	1.990e-06	1.060e+05	1.800e-02	1.066e-03
Ethanol	1.650e+02	3.200e-04	4.971e-01	8.249e-07	7.001e+04	1.500e-02	1.345e-03

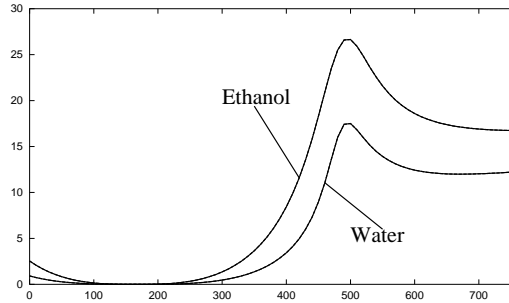
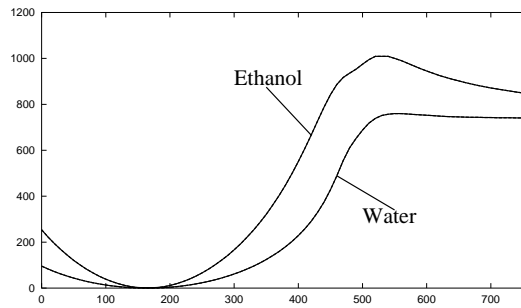
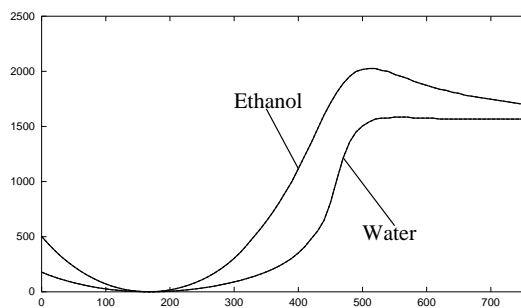
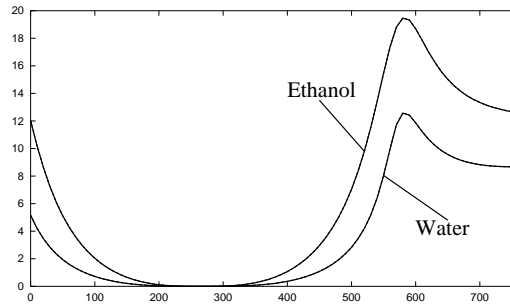
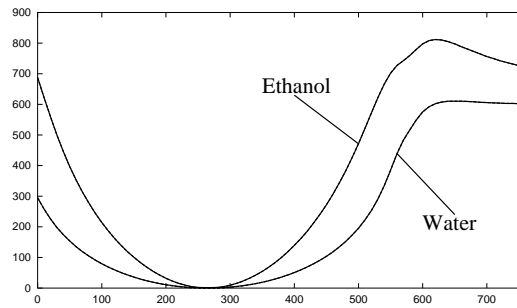
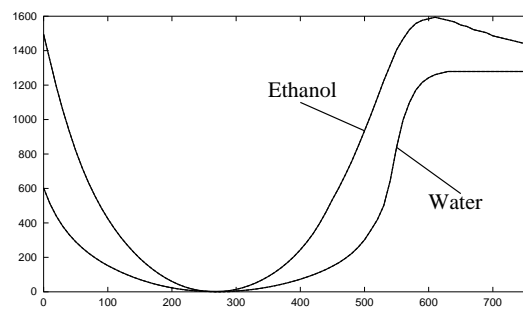
(a) The maximum growth rate  $\omega_{Im}$  versus  $U_\ell$ .(b) The maximum growth rate  $\omega_{Im}$  versus  $U_\ell$ .(c) The cut off wave number  $k_c$  versus  $U_\ell$ .Figure 12.3: KH instability of liquid jet with  $U_\ell$  in compressible gas of  $U_a = 165$  m/s and  $0 < U_\ell < 800$  m/sec.  $n = 0$  solid lines,  $n = 1$  dashed lines. The solid line ( $n = 0$ ) overlaps with the dashed line ( $n = 1$ ).

Table 12.5: Parameters for  $U_a = 265$  m/s.

fluid	$U_a$ (m/sec)	$D_\ell$ (m)	$Ma$	$We$	$Re$	$m$	$\ell$
Water	2.650e+02	3.200e-04	8.316e-01	2.158e-06	1.018e+05	1.800e-02	8.698e-04
Ethanol	2.650e+02	3.200e-04	8.316e-01	8.947e-07	6.722e+04	1.500e-02	1.097e-03

(a) The maximum growth rate  $\omega_{Im}$  versus  $U_\ell$ .(b) The maximum growth rate  $\omega_{Im}$  versus  $U_\ell$ .(c) The cut off wave number  $k_c$  versus  $U_\ell$ .Figure 12.4: KH instability of liquid jet with  $U_\ell$  in compressible gas of  $U_a = 265$  m/s.  $n = 0$  solid lines,  $n = 1$  dashed lines. The solid line ( $n = 0$ ) overlaps with the dashed line ( $n = 1$ ).



### 13 Convective/absolute (C/A) instability

C/A instability is used to determine when the spatial theory of instability makes sense. Practically, this comes down to a determination of the conditions under which a disturbance from a localized source will propagate downstream without corrupting the source. The disturbance may grow as it propagates but after it passes over a fixed point it leaves the flow undisturbed. This is the case for convectively unstable flows, but absolutely unstable flows propagate both upstream and downstream. Propagation of disturbances from a vibrating ribbon in a boundary layer or Poiseuille flow are examples. For such propagation these flows must be convectively and not absolutely unstable.

The study of stability of disturbances issuing from a fixed source, leading to C/A theory, is not a complete stability theory; the traditional temporal theory of instability needs also to be considered. The temporal theory determines the conditions under which disturbances at a fixed point will grow or decay. If these conditions are such that all disturbances decay is stable, then disturbances from a fixed point will decay. Disturbances which are convectively or absolutely unstable are also temporally unstable. The propagation of impulses from a source in a convectively unstable flow can be realized provided the growth rates and amplitudes of temporally unstable flows do not corrupt the flow first. This is why experiments with vibrating ribbons are always done with care to suppress background noise which may amplify in time a fixed point.

Li & Kelly (1992) considered the convective and absolute instability of an inviscid liquid jet in an air stream of an inviscid compressible gas. They motivated their study by experiments on the instability and breakup of liquid fuel jets in crossflow. They note that

“... the breakup of the jet, however, does not seem to proceed in the gradual manner typical of the capillary instability of a liquid jet issuing into air at rest. Here the jet gradually bends over toward the direction of the free stream so that both tangential and cross-flow components of the gas flow are seen by the jet. When the jet is at an angle of about  $30^\circ$  from the normal to the free stream, the jet breaks into large columns in a manner so sudden that Schetz and co-workers (Sherman & Schetz (1971), Schetz *et al.* (1980)) have used the phrase “fracture” to describe the phenomenon. At this angle, the component of the gas velocity parallel to the jet’s direction is approximately sonic ...”

Li & Kelly (1992) did not study a jet in crossflow; they studied a liquid in a coflowing air stream. They also considered the convective and absolute instability of a plane jet and found transition to absolute instability in the transonic region. They speculate that fracture coincides with the transition to absolute instability.

The problem considered by Li & Kelly (1992), C/A instability of a plane jet, is rather far from experiments on cross flow of Sherman & Schetz (1971) and it could be considered in the frame of temporal combined Rayleigh-Taylor, Kelvin-Helmholtz instability which should show rather exceptional behavior in transonic flow. This kind of explanation of rapid breakup of a coflowing jet was given by Varga *et al.* (2003) and it is based on a secondary RT instability not associated with absolute instability.

### 14 Conclusions

We studied the temporal instability of a liquid jet in a high speed compressible air stream using viscous potential flow. Since the shear stress is ignored in viscous potential flow, the analysis is compatible with the discontinuous profile used in all studies of Kelvin-Helmholtz instability. This discontinuity is not allowable for real viscous fluids where shear layers develop. Disturbances with high wavenumbers might see the details of the shear layer and alter the stability results in ways which are presently unknown.

In our analysis, which neglect shear layers, this instability is dominated by capillarity when the Weber number is large and by Kelvin-Helmholtz instability when the Weber number is small. The peak growth rates and the associated wave lengths depend strongly on the Mach number and on the viscosity of the liquid. The growth rates are dramatically larger in the transonic region and the wave lengths of the peak values are much smaller. Viscosity reduces the magnitude of the growth. The growth rate for inviscid potential flow monotonically increases as Mach number increases. For  $0 < \mu_\ell < 0.168$  cP, the growth rate for viscous potential flow monotonically increases as Mach number increases. For  $0.168 \text{ cP} < \mu_\ell$ , the growth rate for viscous potential flow has a peak value when Mach number is nearly one. For more viscous liquids, the growth rate for viscous potential flow has a peak value when Mach number is nearly one. The peak value decreases as the viscosity  $\mu_\ell$  increases. The growth rates are very sharply peaked near  $M_a = 1$  when the viscosity is larger than some value near 0.2 cP. The dramatic change in stability of liquid jets in transonic flow predicted by analysis

is possibly related to the dramatic increases in the drag coefficient of spheres and disks in transonic flow observed in experiments (Howarth (1953), p.724). It is not known if jet breakup in transonic and supersonic flow is caused directly by KH instability or through a secondary RT instability. In either case, this analysis suggests that the drop fragments would be very small.

**Acknowledgement** This work was supported by the NSF/CTS-0076648, the Engineering Research Program of the Office of Basic Energy Sciences at the DOE.

## References

- Batchelor, G.K. & Gill, A.E. 1962. Analysis of the stability of axisymmetric jets, *J.Fluid Mech.*, **14**, 529-551.
- Chang, I.-D. & Russel, P.E. 1965. Stability of a liquid layer adjacent to a high-speed gas stream. *Phys. Fluids*, **8**, 1018-1026.
- Chawla, T.C. 1975. The Kelvin-Helmholtz instability of the gas-liquid interface of a sonic gas jet submerged in a liquid. *J.Fluid Mech.*, **67**, 513-537.
- Chen, T. & Li, X. 1999. Liquid jet atomization in a compressible gas stream, *J.Propulsion and Power* **15**, 369-376.
- Dunne, B. & Cassen, B. 1954. Some phenomena associated with supersonic liquid jets. *J.Appl. Phys.* **25**, 569-572.
- Dunne, B. & Cassen, B. 1956. Velocity discontinuity instability of a liquid jet. *J. Appl.Phys.* **27**, 577-582.
- Engel, O.G. 1958. Fragmentation of waterdrops in the zone behind an air shock. *J.Res.Natl.Bur. Stand.* **60**, 245-280.
- Funada, T. & Joseph, D.D. 2001. Viscous potential flow analysis of Kelvin–Helmholtz instability in a channel, *J.Fluid Mech.*, **445**, 263-283.
- Funada, T. & Joseph, D. D. 2002. Viscous potential flow analysis of capillary instability, *Int. J. Multiphase Flow*, **28**, 1459-1478.
- Funada, T., Joseph, D.D. & Yamashita, S. 2004. Stability of a liquid jet into incompressible gases and liquids. *Int.J. Multiphase Flow*, **30**, 1279-1310.
- Howarth, L. 1953. *Modern developments in fluid dynamics: high speed flow*. Clarendon Press, Oxford.
- Joseph, D.D. 2003. Viscous potential flow, *J. Fluid Mech.*, **479**, 191-197.
- Joseph, D.D., Belanger, J. & Beavers, G.S. 1999. Breakup of a liquid drop suddenly exposed to a high-speed airstream, *Int. J. Multiphase Flow* **25**, 1263-1303.
- Joseph, D. D., Beavers G. S. & Funada, T. 2002. Rayleigh–Taylor instability of viscoelastic drops at high Weber numbers, *J. Fluid Mech.*, **453**, 109-132.
- Joseph, D.D. 1976. *Stability of Fluid Motions, I and II*. Springer Tracts in Natural Philosophy. vol.27 and 28. Berlin-Heidelberg-New York:Springer-Verlag.
- Li, H.-S. & Kelly, R.E. 1992. The instability of a liquid jet in a compressible airstream. *Phys. Fluids A* **4**, 2162-2168.
- Lin, S.P. 2003. *Breakup of Liquid Sheets and Jets*. Cambridge University Press.
- Nayfeh, A.H. & Saric, W.S. 1973. Nonlinear stability of a liquid film adjacent to a supersonic stream, *J.Fluid Mech.*, **58**, 39-51.
- Schetz, J.A., Kush, E.A. & Joshi, P.B. 1980. Wave phenomena in liquid jet breakup in a supersonic crossflow. *AIAA J.* **18**, 774-778.
- Sherman, A. & Schetz, J.A., 1971. Breakup of liquid sheets and jets in a supersonic gas stream, *AIAA J.* **9**, 666-673.

- Theofanous, T.G., Li, G.J. & Dinh, T.N. 2003. Aerobreakup in rarefied supersonic gas flows, Proceedings of FEDSM03 4-th ASME/JSME Joint Fluids Engineering Conference.
- Varga, C.M., Lasheras, J.C. & Hopfinger, E.J. 2003. Initial breakup of a small-diameter liquid jet by a high-speed gas stream, *J.Fluid Mech.*, **497**, 405-434.
- Zhou, Z.W. & Lin, S.P. 1992. Absolute and convective instability of a compressible jet, *Phys. Fluids* **A4**, 277-282.